Elastic relaxations associated with the $Pm\bar{3}m$–$R\bar{3}c$ transition in $LaAlO_3$: III. Superattenuation of acoustic resonances

2010 J. Phys.: Condens. Matter 22 035405

(http://iopscience.iop.org/0953-8984/22/3/035405)

J. Phys.: Condens. Matter **22** (2010) 035405 (19pp) doi:10.1088/0953-8984/22/3/035405

Elastic relaxations associated with the $Pm\bar{3}m$–$R\bar{3}c$ transition in $LaAlO_3$: III. Superattenuation of acoustic resonances

M A Carpenter[1], A Buckley[1], P A Taylor[1] and T W Darling[2,3]

[1] Department of Earth Sciences, University of Cambridge, Downing Street, Cambridge CB2 3EQ, UK
[2] Material Science and Technology, Los Alamos National Laboratory, Los Alamos, NM 87545, USA
[3] Department of Physics, University of Nevada, Reno, NV 89577, USA

E-mail: mc43@esc.cam.ac.uk

Received 1 August 2009, in final form 13 November 2009
Published 21 December 2009
Online at stacks.iop.org/JPhysCM/22/035405

Abstract

Resonant ultrasound spectroscopy has been used to characterize elastic softening and anelastic dissipation processes associated with the $Pm\bar{3}m \leftrightarrow R\bar{3}c$ transition in single crystal and ceramic samples of $LaAlO_3$. Softening of the cubic structure ahead of the transition point is not accompanied by an increase in dissipation but follows different temperature dependences for the bulk modulus, $\frac{1}{3}(C_{11} + 2C_{12})$, and the shear components, $\frac{1}{2}(C_{11} - C_{12})$ and C_{44}, as if the tilting instability contains two slightly different critical temperatures. The transition itself is marked by the complete disappearance of resonance peaks (superattenuation), which then reappear below ~700 K in spectra from single crystals. Comparisons with low frequency, high stress data from the literature indicate that the dissipation is not due to macroscopic displacement of needle twins. An alternative mechanism, local bowing of twin walls under low dynamic stress, is postulated. Pinning of the walls with respect to this displacement process occurs below ~350 K. Anelasticity maps, analogous to plastic deformation mechanism maps, are proposed to display dispersion relations and temperature/frequency/stress fields for different twin wall related dissipation mechanisms. These allow comparisons to be made of anelastic loss mechanisms under mechanical stress with elastic behaviour observed by means of Brillouin scattering at high frequencies which might also be related to microstructure.

1. Introduction

Many important electroceramics with high permittivity, strong electric polarization or large piezoelectric coupling coefficients are based on crystalline materials with the perovskite structure. Technological applications often involve some element of switching, and the dynamic behaviour of these materials under the influence of a cyclical stress or electric field has been the subject of intensive research. Because the most advantageous properties tend to be developed in crystals which undergo multiple phase transitions and characteristically contain ferroelastic twin walls, an observed dynamic response may in fact be determined largely by the dynamic response of the twin walls rather than of the bulk material. In particular, movement of the walls can give rise to large strains and anelastic dissipation. This aspect of the behaviour of materials such as PZT has been investigated by mechanical spectroscopy over a prolonged period (Postnikov *et al* 1970, Wang *et al* 2001, 2002, 2006, Bourim *et al* 2002). In purely ferroelastic perovskites, the mobility of twin walls can become the dominant factor in determining the response to an applied stress. For example, easy twin wall motion in $SrTiO_3$ below the $Pm\bar{3}m \leftrightarrow I4/mcm$ transition, at frequencies of ~10–50 Hz, can reduce the effective values for selected elastic moduli to only ~30% of their values in the stability field of the cubic structure (Schranz *et al* 1999, Kityk *et al* 2000a, 2000b, Lemanov *et al* 2002). This superelastic response at low frequencies has been seen in $KMnF_3$ (Schranz *et al* 2003, Schranz and Kityk 2008, Salje and Zhang 2009), (Ca, Sr)TiO_3 (Harrison *et al* 2003), (Sr, Ba)SnO_3 (Daraktchiev *et al* 2006,

2007) and $LaAlO_3$ (Harrison and Redfern 2002, Harrison *et al* 2004c, 2004b). The influence of twin wall mobility is seen also in strong acoustic dissipation, which has potential implications for the attenuation of seismic waves by silicate perovskites in the earth's lower mantle (Harrison and Redfern 2002). Such mobility is not restricted to low frequencies of applied stress, however, and can be detected in $SrTiO_3$ at frequencies as high as ~200 MHz (Rehwald (1970), Rehwald (1971), and see compilation of data in Carpenter (2007)). The question then arises as to whether a single relaxation mechanism applies to all twin walls or whether a diversity of mechanisms can operate at different temperatures, pressures and frequencies such that there could be a richness of anelastic behaviour comparable to that of plastic deformation.

Against this wider background, the present study was designed to investigate the elastic and anelastic properties of single crystal and ceramic samples of $LaAlO_3$ at frequencies of 0.3–2 MHz by resonant ultrasound spectroscopy (RUS) from 10 K, through the $Pm\bar{3}m \leftrightarrow R\bar{3}c$ transition at $T_c \approx$ 820 K and up to 1100 K in the stability field of the cubic structure. Migliori *et al* (1993) have previously reported that 'RUS is so sensitive to macroscopic twinning that useable data of any sort often cannot be obtained in a twin sample because of substantial degradation of resonance signals'. Such strong dissipation effects can become a serious problem if the objective is to measure absolute values of elastic moduli or to follow their variations with temperature. On the other hand, if the objective is to understand the dynamical mechanical properties of twin walls, such sensitivity to dissipation processes provides unique and unexploited opportunities.

A great deal is already known about twin wall dynamics in $LaAlO_3$ from the work of Harrison and co-workers (Harrison and Redfern 2002, Harrison *et al* 2004c, 2004b). Large strains arise by displacement of the tips of needle twins over mm length scales when an alternating stress is applied at frequencies of between ~0.01 and ~50 Hz. Superelastic softening and high dissipation was found to occur over a wide temperature interval from ~500 K to T_c. A large peak in the attenuation and a steep increase in the effective elastic modulus between ~370 and ~470 K was ascribed to pinning of the twin walls by defects. Essentially the same single crystal material has been examined by RUS in the present study and a temperature interval of ~100 K below T_c has been found in which all acoustic resonance disappear completely. Because of the apparent association of this behaviour with the temperature interval of superelastic softening at low frequencies the complete disappearance of resonance peaks is being referred to as superattenuation (Carpenter *et al* 2006). Values of the elastic moduli, to exclude the influence of twin walls, have been determined from room temperature to ~1000 K by Brillouin spectroscopy, and the influence of the $Pm\bar{3}m \leftrightarrow R\bar{3}c$ transition has been described using Landau theory (Carpenter *et al* 2010c, 2010b). Additional softening beyond that expected on the basis of strain/order parameter coupling alone, at high temperatures in the stability field of the rhombohedral structure, appears to be due to coupling between acoustic modes and a central peak mode. The origin of the central peak has been ascribed to a combination of phonon density fluctuations and flipping of clusters of tilted octahedra between different ⟨111⟩, ⟨011⟩ and ⟨001⟩ axes (Carpenter *et al* 2010b). In this temperature interval, the twin wall widths also become wider than ~50–100 Å (Chrosch and Salje 1999) and a variety of other anomalies appear in the evolution of strain parameters and optic phonon frequencies (Hayward *et al* 2005).

The present paper is divided into five sections. Following this introduction, the experimental samples and RUS methodology used for data collection and analysis are described in section 2. Extensive sets of elastic moduli and acoustic dissipation data are presented in section 3. The focus of the discussion (section 4) is then on comparisons with elasticity data from low frequency measurements made by dynamical mechanical analysis and from high frequency measurements made by Brillouin scattering. In combination, the data from three different frequency ranges provide evidence of previously unrecognized relaxational behaviour due to both extrinsic effects, such as the mobile twin walls, and intrinsic effects, such as possible static/dynamic disordering of atomic positions at low temperatures. A synthesis of the possible behaviour of twin walls, in terms of creep and sliding mechanisms for different types of domain wall motion, is presented in the form of anelasticity maps which show the dependence on frequency, stress and temperature. A brief summary of the results from the first three papers in this series (including Carpenter *et al* 2010c, 2010b) is given in section 5. Observations of the elastic behaviour below room temperature are presented in a subsequent paper (Carpenter *et al* 2009a).

2. Experimental methods

2.1. Sample preparation

Rectangular parallelepipeds were prepared from the same Czochralski-grown single crystal of $LaAlO_3$ as used to provide crystals for GHz ultrasonic measurements (Carpenter *et al* 2010c) and Brillouin spectroscopy (Carpenter *et al* 2010b). The 44 g pale pink crystal originally purchased from Crystal Gmbh (Berlin) came with two faces parallel to (100). Rectangular parallelepipeds with faces parallel to {100} were cut from it using a fine (~300 μm) annular diamond saw lubricated with paraffin. This gave smooth, closely parallel faces, and no further surface preparation was required. Crystallographic orientations were checked using a back reflection Laue x-ray camera, and the faces were estimated to be within ±~1° of the pseudocubic crystallographic axes. Rhombohedral distortion of the $LaAlO_3$ structure gives rise to a deviation of unit cell angles from 90° of only ~0.1° at room temperature (Hayward *et al* 2005), which is well below the uncertainty in the alignment arising during cutting of the parallelepipeds.

Four single crystal parallelepipeds were used for RUS measurements; their dimensions and masses are listed in table 1. A slight discrepancy was found between the density of the parallelepipeds calculated from their masses and measured dimensions, 6.31(4/2002), 6.42 (2/2003), 6.31 (4/2002), 6.47 (1/2003) g cm^{-3}, and the density of 6.526 ± 0.003 g cm^{-3}

Table 1. Dimensions, masses and room temperature elastic moduli of parallelepipeds used for RUS measurements. LA = Los Alamos high temperature instrument. C = Cambridge high temperature instrument.

Sample no.	Dimensions (mm)	Mass (g)	Density from measured dimensions (g cm^{-3})	$\frac{1}{2}(C_{11}-C_{12})$ (GPa)	C_{44} (GPa)	K (GPa)	Rms error on fit (%)
1/2002 (before heating, LA)	4.952 5.383 5.925	1.0103	6.40	60.7	145.5	219.1	0.6
1/2002 (after heating, LA)				59.8	146.1	245.0	1.2
4/2002 (before heating, C)	3.906 4.440 4.808	0.5263	6.31	61.4	145.9	209.1	0.4
4/2002 (after heating, C)				60.9	145.1	211.8	0.5
1/2003 (before heating, LA)	4.994 5.483 5.997	1.0622	6.47	60.3	147.9	230.1	0.7
1/2003 (after heating, LA)				59.3	146.7	297.5	1.0
2/2003 (before heating, C)	5.024 5.484 5.998	1.0615	6.42	59.9	148.2	231.4	0.9
cer1 (before heating, C)	2.660 3.148 3.624	0.1648	5.43	45.2		86.2	0.6
cer1 (after heating, C)		0.1641	5.41	45.2		83.9	0.6

obtained for a much larger piece of the original crystal by the Archimedes method (Carpenter *et al* 2010c). This was most probably due to errors in the measured linear dimensions associated with deviations of the parallelepipeds from perfectly rectangular cross sections.

Two ceramic parallelepipeds were prepared from $LaAlO_3$ powder by crushing offcuts left after sawing up the large single crystal. The powder was sieved and washed to produce grains with sizes in the range 10–40 μm for the neutron powder diffraction experiment described by Hayward *et al* (2005). As part the neutron data collection, it had been heated up to 1270 K in a vacuum of $\sim 10^{-3}$ mbar which left the grains with a grey colour. The powder was annealed in air at 1000 °C for ~18 h to restore the original pinkish colour and approximately 5 g was pressed into a pellet using a 12 mm bore infrared pellet die. The pellet was then fired at 1600 °C for 48 h, with a ramp rate of 10 °C min^{-1} for heating and cooling. Parallelepipeds with dimensions 2.660 × 3.148 × 3.624 mm^3, mass 0.1648 g (cer1) and 2.662 × 3.150 × 3.668 mm^3, 0.1665 g (cer2) were sawn from the resulting pink/brown sample and used for RUS. The density given by these dimensions is 83% of the theoretical density calculated from lattice parameters and stoichiometric unit cell contents.

2.2. RUS data collection

The RUS method has been described in detail elsewhere (Migliori *et al* 1993, 2001, Maynard 1996, Leisure and Willis 1997, Migliori and Sarrao 1997, Zadler *et al* 2004, Lakes 2004, Migliori and Maynard 2005). High temperature RUS experiments for the present study were first undertaken in Los Alamos using an instrument initially designed for *in situ* analysis of heat treatment in steels. The RUS head was supported within a horizontal silica glass tube with diameter 75 mm which, in turn, was enclosed in a horizontal resistance furnace. Ultrahigh purity (>99.99%) argon gas at slightly over atmospheric pressure was passed through the tube to prevent oxidation of the metal parts of the RUS assembly. Some of the components were made of graphite, and the sample was therefore exposed to a reducing environment at high temperatures. Temperature was monitored with a type K thermocouple placed close to the sample. The single crystal parallelepiped 1/2002 was placed across its corners directly on $LiNbO_3$ transducers and spectra were collected at temperatures up to 916 K using DRS Modulus II system driving electronics. The driving voltage was increased by a broadband 5:1 transformer between the DRS output and the transducer, and at high temperatures a series capacitor of 100 pf decoupled the DC voltages introduced by charge carrier excitation in the $LiNbO_3$. Sample 1/2003 was used in a second run. Spectra were collected in 4 separate 0.17 MHz segments across a frequency range of 0.20–0.85 MHz. There were 500 data points per segment, corresponding to a resolution in frequency of 0.34 kHz.

Further single crystal data collections were completed on RUS instruments with dynamic resonance system (DRS) Modulus II electronics in Cambridge, using parallelepipeds 4/2002 and 2/2003. In the high temperature system the parallelepiped rested across its corners between the tips of alumina rods which extended into a horizontal Netzsch 1600 °C furnace, with the transducers located outside the furnace on the other end of the rods (McKnight *et al* 2008). The thermocouple used to monitor temperature was located within a few mm of the sample. In separate experiments, the transition temperature of a single crystal of quartz was found to be ~3 K above the expected temperature of 846 K, indicating that the thermocouple readings were slightly high at this temperature (McKnight *et al* 2008, 2009a). As discussed below, a slight rescaling of the measured temperatures to give corrected temperatures was required, therefore. Sets of spectra

were first collected in sequences with each temperature set manually and then in automated heating or cooling sequences, driven by software produced in-house. Spectral ranges within the limits 0.2–1.2 MHz were usually used, with 50 000 data points per spectrum. These provided a resolution in frequency of 0.02 kHz or better. The system used to collect spectra below room temperature, in which the sample is held lightly between PZT transducers has been described by McKnight *et al* (2007).

Room temperature spectra were collected before and after heat treatment using separate RUS heads in Los Alamos and Cambridge. Each of the parallelepipeds was mounted and remounted several times in different orientations to ensure that all resonance peaks were detected.

RUS spectra from the ceramic parallelepiped cer1 were collected in the Cambridge high temperature and low temperature instruments, using automated heating and cooling cycles, with similar instrument settings to those used for the single crystal data sets: 0.2–1.2 MHz above room temperature with 50 000 data points per spectrum, 0.3–1.8 MHz below room temperature with 100 000 data points per spectrum.

2.3. RUS data analysis

All the spectra were analysed offline within the software package 'Igor Pro' (Wavemetrics). Peak frequencies in spectra from the single crystal parallelepipeds were measured by inspection and used to calculate the cubic moduli, $\frac{1}{2}(C_{11} - C_{12})$, C_{44}, and bulk modulus, K, using the DRS software described by Migliori and Sarrao (1997). Values determined from the room temperature spectra were used as starting parameters for fitting of frequencies from spectra collected up to ~570 K. Elastic moduli from the Brillouin data of Carpenter *et al* (2010b) were used as starting parameters for fitting to sets of peak frequencies collected in the stability field of the cubic structure. Lattice parameter data of Hayward *et al* (2005) were used to correct the dimensions of the parallelepipeds for the influence of thermal expansion at both high and low temperatures. This procedure resulted in fits with rms errors of 0.2–0.3% for the cubic phase and 0.4–0.9% for the rhombohedral phase. The former constitute 'good' fits (Migliori and Sarrao 1997, Migliori and Maynard 2005), while the latter indicate that the rhombohedral crystals departed from average cubic geometry even though they contained abundant transformation twins. The χ^2 matrix for individual elastic moduli showed that the (average) cubic shear elastic moduli, '$\frac{1}{2}(C_{11} - C_{12})$' and '$C_{44}$', were tightly constrained by the data. (Quotation marks are used here and below to emphasize that these are from cubic fits to the resonance frequencies.)

Values of K and the shear modulus, G, for polycrystalline $LaAlO_3$ in the stability field of the $Pm\bar{3}m$ structure were determined in the same way using peak frequencies from spectra for the ceramic parallelepiped cer1. Repeat runs were undertaken with the parallelepiped set in different orientations to ensure that all resonance peaks were found. Rms errors were ~0.6–0.8%, with the greatest uncertainty being for K. The slightly less than 'good' fits are assumed to be due to anisotropy of grain orientations or to an anisotropic distribution of pore sizes/orientations.

Peak positions and widths were also determined for selected peaks in the RUS spectra from the Cambridge instrument by fitting with an asymmetric Lorentzian function, analogous to the approach described by Schreuer *et al* (2003) and Schreuer and Thybaut (2005). The Los Alamos spectra had been collected at lower resolution in frequency, and peak widths were estimated by printing relevant segments and measuring the peaks manually. Values of the mechanical quality factor, Q, were determined as $Q = f/\Delta f$, where f is the peak frequency and Δf is the peak width at half maximum height. The inverse quality factor, Q^{-1}, is a measure of acoustic dissipation within the sample. Small discontinuities in the temperature dependence of these values occur at room temperature because of slight differences in the peak widths obtained when the crystal sits directly on the piezoelectric transducer (in the cryostat) and when it is separated from the transducers by alumina rods (Cambridge furnace). These differences are much smaller than the overall variations with temperature.

3. Results

3.1. Elastic moduli at room temperature

Room temperature moduli for the four single crystal parallelepipeds were determined using up to 78 peak frequencies, giving '$\frac{1}{2}(C_{11} - C_{12})$' values in the range 59.3–61.4, 'C_{44}' values in the range 145.1–148.2 and values of K in the range 209.1–245.0 GPa (table 1). These are average values for the combination of rhombohedral twins present in the crystals but are not far from the values $\frac{1}{2}(C_{11} - C_{12}) = 68.3$, $C_{44} = 149.0$ GPa obtained for a single twin domain by Brillouin scattering (cubic setting of rhombohedral phase in table 4 of Carpenter *et al* (2010c)). Scatter in values of the shear elastic moduli does not correlate with the density calculated from the parallelepiped dimensions and masses, implying that uncertainties in shape were not the main source of uncertainty in the RUS data. Peak frequencies measured at room temperature for the single crystal parallelepipeds shifted slightly after they had been heated in the stability field of the cubic structure and cooled back to room temperature. This is most likely due to a change in twin configuration upon heating and then cooling back through the phase transition temperature, implying that twin configurations play a role in determining the average cubic moduli of the individual crystals. Values of the shear elastic moduli obtained from room temperature spectra collected after heating remained in the same ranges as they were before heating for all the samples, however (table 1). Values of K from the fits were poorly constrained by the data, had a large scatter between samples, and were substantially greater than the Voigt/Reuss/Hill value of 195.4 GPa obtained by Brillouin scattering. The origin of this discrepancy lies in the fact that the single crystals have specific crystallographic orientations, which might give average cubic geometry but are not random in the Voigt/Reuss/Hill sense.

Parallelepipeds 4/2002 and 2/2003 heated in air in the Cambridge high temperature instrument emerged with the

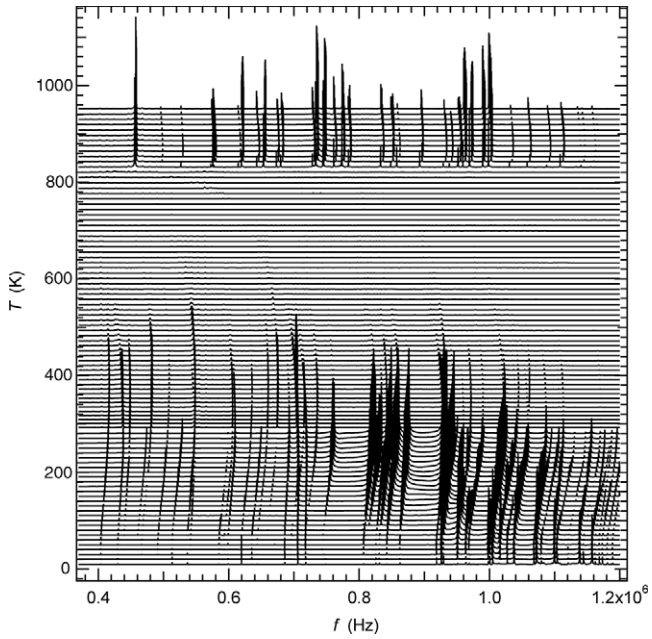

Figure 1. A complete stack of RUS spectra from a single crystal of $LaAlO_3$, at ∼10 K intervals from ∼10 to ∼950 K (crystal 4/2002). The y-axis is amplitude but the spectra have been displaced in proportion to the temperature at which they were collected and the axis is labelled as temperature. During cooling, the onset of superattenuation of acoustic resonances is associated with the cubic → rhombohedral transition, near ∼820 K. Broad, weak resonance peaks reappear below ∼600 K and become progressively sharper and stronger with further cooling.

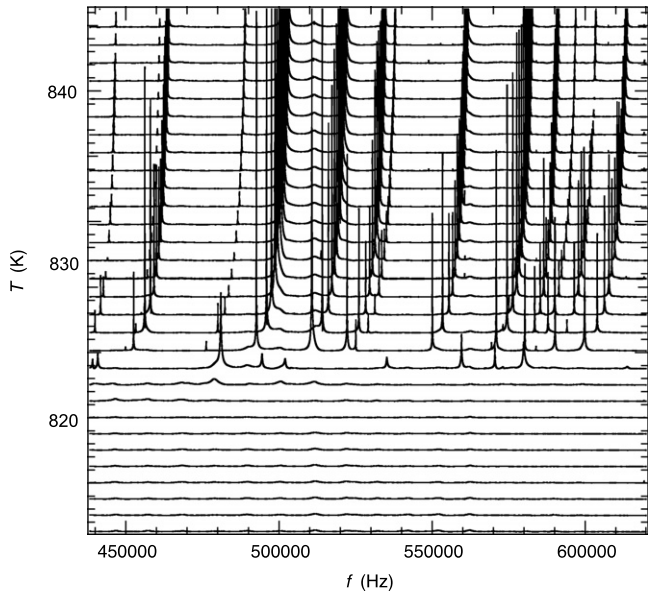

Figure 2. Part of a stack of RUS spectra at ∼1 K intervals through the cubic → rhombohedral transition (single crystal 2/2003). The y-axis is amplitude but the spectra have been displaced in proportion to the temperature at which they were collected and the axis is labelled as temperature. During cooling, the last resonance peaks from the sample are seen at 822 K (before recalibration of the temperature scale). Weak peaks showing no temperature dependence below 822 K are instrumental noise.

same pink colour that they had had at the start. The colour of parallelepipeds 1/2002 and 1/2003 was grey after they had been heated in the reducing atmosphere of the Los Alamos high temperature instrument, but this did not produce an obviously systematic change in the values of their shear elastic moduli at room temperature.

A fit to 50 peak frequencies obtained at room temperature from the ceramic sample before heating yielded $G = 45.2$ and $K = 86.2$ GPa, assuming that it was isotropic. Peak frequencies remained essentially unchanged after heating to above the cubic ↔ rhombohedral transition temperature, and the values of K and G (table 1) were the same, within experimental uncertainty.

3.2. High temperature spectra from heating in air, Cambridge

Figure 1 shows a set of spectra collected from parallelepiped 4/2002 during heating in four segments, ∼10–300, ∼290–380, ∼370–620 and 620–950 K, with temperature steps of ∼10 K and an equilibration time of 15 min before data collection at each temperature. Heating from 10 K at first caused resonance peaks to increase in frequency, corresponding to increasing elastic stiffness, but this trend reversed above ∼400 K. The lowering of resonance frequencies above ∼400 K (elastic softening) was accompanied by line broadening and diminishing intensity. The peaks seemed to disappear from spectra collected at ∼580 K and above, though close inspection showed residual peaks perhaps up to ∼680 K. Spectra collected between ∼680 and ∼820 K contained no obvious resonance peaks. Narrow peaks reappeared in spectra collected at ∼830 K and above.

Figure 2 contains details of a sequence of spectra collected from sample 2/2003 at 1 K steps during heating through the range 808–856 K, with an equilibration time of 15 min at each temperature. This shows a complete absence of peaks at 821 K, some possible weak peaks at 822 K, and narrow, strong peaks at 823 K and above. Cooling of the crystal through the same temperature interval, again with data collection every 1 K, gave essentially the same result. As noted above, a calibration test of the furnace temperatures gave the sharp minimum in elastic moduli of quartz at a few degrees above the α–β transition temperature of 846 K. In the entirely separate experiment in Los Alamos, described below, sharp resonance peaks were detected at 818 K but not at 816 K. This coincides closely with the transition temperature of 817 K for the $Pm\bar{3}m$–$R\bar{3}c$ transition used by Carpenter *et al* (2010b). An adjustment of temperatures from the Cambridge high temperature RUS furnace was therefore applied to all the following results such that the observed temperature (T_{obs}) of 821 K has been rescaled to 817 K according to $T = 2.265 + 0.9924T_{obs}$.

Figure 3 contains details of five peaks in spectra collected from sample 2/2003 with 20 K steps in a heating sequence, and shows the frequency shifts plus line broadening with increasing temperature. The DRS software used for fitting elastic moduli indicated that the frequencies of distortional modes responsible for the first four of these were determined by 99–100% of $\frac{1}{2}(C_{11} - C_{12})$', while the mode responsible for the peak at ∼0.42 MHz was determined by 92% of 'C_{44}'. From this,

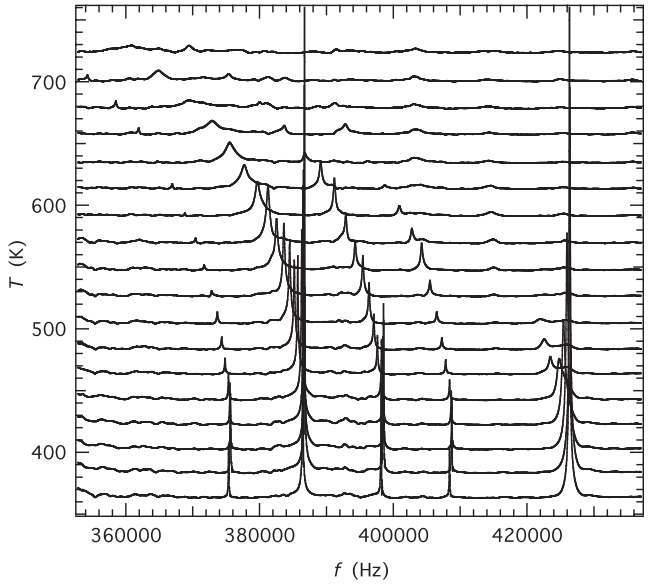

Figure 3. Part of a stack of RUS spectra at ∼20 K intervals through the temperature interval of continuous onset of superattenuation (single crystal 2/2003). The y-axis is amplitude but the spectra have been displaced in proportion to the temperature at which they were collected and the axis is labelled as temperature. The four peaks with lowest resonance frequencies depend predominantly (∼92–100%) on '$\frac{1}{2}(C_{11} - C_{12})$'. The peak at ∼0.43 MHz depends predominantly (∼92%) on 'C_{44}'. With increasing temperature, softening and broadening of the peaks occurs; the 'C_{44}' peak is the first to disappear completely from the spectra.

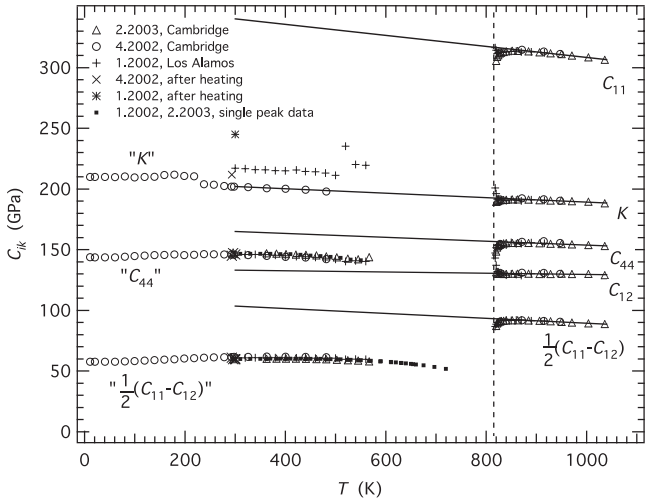

Figure 4. Values of elastic moduli obtained from single crystal RUS spectra. The temperature scale has been adjusted to give the $Pm\bar{3}m \leftrightarrow R\bar{3}c$ transition at 817 K (vertical dashed line). Straight lines fit to the cubic data between 885 and 1036 K have been extrapolated to lower temperatures in order to emphasize the elastic softening which arises as a consequence of the phase transition. Symbols below T_c are from fits to resonance peak frequencies, using average cubic moduli. Data for K below room temperature are poorly constrained by the resonance frequencies. Square dots represent values obtained by calibration of the frequencies of single peaks for 'C_{44}' and '$\frac{1}{2}(C_{11} - C_{12})$'.

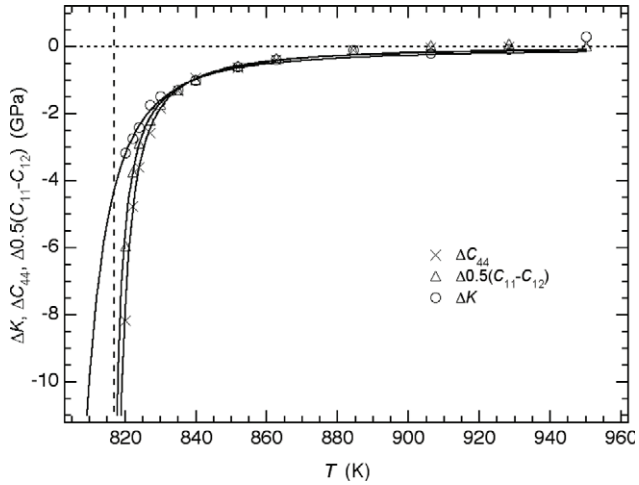

Figure 5. Pretransitional softening in single crystal $LaAlO_3$, as given by the difference between linear extrapolation of fits to data above 885 K (straight lines in figure 4) and observed values of the elastic moduli. Curves are fits of equation (11) to the data using $T_c = 815$ K for ΔC_{44} and $\Delta(\frac{1}{2}(C_{11} - C_{12}))$ and $T_c = 797$ K for ΔK. The vertical dashed line is at 817 K.

and from equivalent observations of other peaks in spectra from different crystals, it is apparent that peaks associated with 'C_{44}' broadened and then disappeared at systematically lower temperatures than peaks associated with '$\frac{1}{2}(C_{11} - C_{12})$'.

Values of moduli obtained from fits to peak frequencies for both of samples 2/2003 and 4/2002 are listed in table 2 and shown in figure 4, using the corrected temperature scale. Extension of the data for '$\frac{1}{2}(C_{11} - C_{12})$' to temperatures between 590 and 720 K was achieved by first calibrating the square of the peak frequency of a prominent '$\frac{1}{2}(C_{11} - C_{12})$' peak from lower temperatures against the fit values. The calibration was then used to calculate values from the frequencies of that peak alone up to the temperature at which it could no longer be identified in the spectra. These values are shown as dots in figure 4. There is close agreement between all data points collected from three different crystals (including for 1/2002, described below), apart from the values of K below the transition temperature which are widely scattered. In the stability field of the $Pm\bar{3}m$ structure, each of the individual moduli varied linearly with temperature down to ∼40 above 817 K. A small degree of softening then occurred as the transition point was approached, which has been determined as the difference, ΔC_{ik}, from straight line fits to data for a single heating sequence (crystal 2/2003) in the temperature interval 885–1036 K ($C_{11} = 353.84 - 0.045\,39T$, $C_{12} = 134.61 - 0.004\,96T$, $C_{44} = 169.82 - 0.016\,08T$, $K = 207.65 - 0.018\,39T$, $\frac{1}{2}(C_{11} - C_{12}) = 109.61 - 0.020\,21T$). Variations of the symmetry-adapted combinations, $\Delta K = \Delta(\frac{1}{3}(C_{11} + 2C_{12}))$, $\Delta(\frac{1}{2}(C_{11} - C_{12}))$ and ΔC_{44} from this sequence are shown in figure 5; softening of the bulk modulus is slightly different from softening of the shear elastic moduli.

Within the stability field of the rhombohedral structure, values of '$\frac{1}{2}(C_{11} - C_{12})$' and '$C_{44}$' are substantially lower than the extrapolated linear fits to the cubic data, as is characteristic for a second order phase transition with strain relaxation due to strain/order parameter coupling (Carpenter *et al* 2010b). As discussed in more detail in Carpenter *et al* (2009a), both

Table 2. Single crystal elastic modulus data at different temperatures for $LaAlO_3$. Inverted commas indicate average cubic values for the rhombohedral phase.

Sample	T (K)	C_{11} (GPa)	C_{12} (GPa)	C_{44}, 'C_{44}' (GPa)	'$\frac{1}{2}(C_{11} - C_{12})$' (GPa)
2/2003	296.0			147.7	59.8
	362.5			147.0	60.0
	382.4			146.7	60.2
	401.2			146.3	60.2
	421.1			146.0	60.1
	440.9			145.8	60.1
	461.7			145.3	59.8
	481.6			144.5	59.7
	502.4			143.7	59.3
	524.3			142.6	58.8
	545.1			142.1	58.6
	566.9			143.8	58.0
	820.0	305.6	131.4	148.5	
	822.0	308.8	130.3	151.9	
	824.0	310.2	130.1	153.0	
	826.9	311.7	130.3	154.0	
	829.9	312.4	130.1	154.6	
	834.9	312.9	130.0	155.1	
	839.9	313.4	130.1	155.4	
	851.8	313.9	130.2	155.5	
	862.7	313.8	130.2	155.6	
	884.5	313.5	130.2	155.5	
	906.3	312.6	129.9	155.2	
	928.2	311.8	129.9	154.9	
	950.0	311.1	130.2	154.6	
	970.8	309.9	129.9	154.3	
	1003.6	308.5	130.0	153.8	
	1036.4	306.4	129.0	153.0	
	292.5			145.9	61.5
	325.7			145.5	61.7
	363.0			144.8	61.9
	400.2			144.1	61.8
	440.2			143.5	61.6
	481.4			142.3	61.4
	827.5	312.4	130.9	154.7	
	871.2	314.7	131.0	156.4	
	914.6	313.3	130.8	157.0	
	947.3	311.2	130.0	155.6	
1/2002 from complete refinement	300			145.4	60.7
	320			146.0	60.8
	340			146.1	61.0
	360			145.9	60.9
	380			145.4	61.2
	400			145.0	61.0
	422			144.4	60.9
	440			144.2	60.8
	460			143.6	60.7
	480			143.1	60.5
	500			142.0	60.7
	520			140.3	59.7
	540			140.8	59.8
	560			140.4	59.7
	818	316.5	143.1	147.2	
	820	314.4	137.1	151.7	
	822	311.6	131.8	153.7	
	824	312.3	131.8	153.8	
	830	312.8	129.9	153.1	
	840	312.9	129.0	153.8	
	850	313.5	130.1	156.0	
	860	313.7	129.6	154.9	
	870	312.9	128.8	155.0	
	890	313.0	130.2	155.7	
	916	312.2	129.7	155.3	

Table 2. (Continued.)

Sample	T (K)	C_{11} (GPa)	C_{12} (GPa)	C_{44}, 'C_{44}' (GPa)	'$\frac{1}{2}(C_{11} - C_{12})$' (GPa)
1/2002 from calibration of single resonance peaks	310			146.6	59.9
	330			146.6	60.0
	350			146.6	60.1
	370			146.6	60.2
	390			146.3	60.2
	410			146.3	60.2
	430			145.8	60.2
	450			145.2	60.1
	470			144.8	60.0
	490			144.1	59.8
	510			143.2	59.6
	530			141.8	59.3
	550			141.3	59.0
	570				58.5
	590				58.1
	610				57.5
	620				57.2
	630				56.7
	640				56.4
	650				55.9
	660				55.4

'$\frac{1}{2}(C_{11} - C_{12})$' and '$C_{44}$' showed a small but real degree of additional softening as temperature reduced from room temperature down to ∼60 K, before levelling off as $T \rightarrow 0$ K. The total softening was slightly greater for '$\frac{1}{2}(C_{11} - C_{12})$' (∼3.8 GPa) than for '$C_{44}$' (∼2.3 GPa). The large scatter in values of K further emphasizes that the average cubic bulk modulus has not really been constrained for twinned rhombohedral crystals.

3.3. High temperature measurements in argon atmosphere, Los Alamos

Spectra were collected in 20 K steps while parallelepiped 1/2002 was heated at a continuous ramp rate of 3 K min^{-1} from room temperature to 700 K, followed by 2 K steps with a ramp rate of 1 K min^{-1} from 720 to 916 K. The sample was then cooled at 1 K min^{-1} with data collection every 2 K down to 800 K, followed by data collection every 10 K down to room temperature. During heating, the spectra did not change significantly up to ∼400 K but the peaks then started to broaden and reduce in amplitude. By ∼700 K all the peaks had disappeared. No peaks were present in spectra collected at temperatures up to 816 K but the spectrum collected at 818 K contained sharp resonance peaks again. These remained up to the highest temperature reached (916 K). Normal spectra were obtained down to 818 K during the cooling sequence, but there were no peaks in the spectrum collected at 814 K. The 816 K spectrum contained a few irregularities in the baseline which may have been very weak resonance peaks. Broad, weak peaks reappeared at ∼700 K and these sharpened and became more intense down to ∼400 K. Below 400 K there were no further changes visible in the primary spectra. The crystal had been pale pink at the start but was pale grey at the end of the run. Detailed analysis was undertaken of selected spectra collected during the heating and cooling sequences and, although fewer peaks were used and rms errors were slightly larger, values obtained for the elastic moduli were generally in close agreement with the Cambridge data set (figure 4).

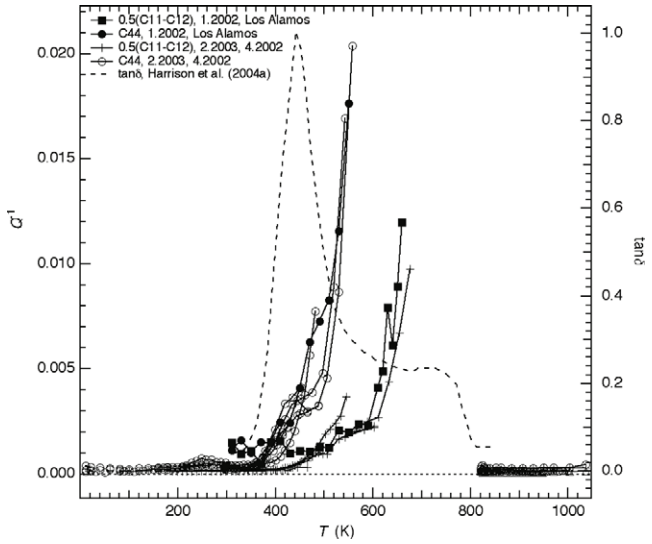

Figure 6. Variation of Q^{-1} as a function of temperature from RUS measurements on single crystals (left axis), together with data for tan δ (right axis) reproduced from figure 2 of Harrison *et al* (2004c). Circles are from resonance peaks which depend primarily on 'C_{44}'; crosses and squares are from peaks which depend on '$\frac{1}{2}(C_{11} - C_{12})$'. Filled symbols represent data obtained from the instrument in Los Alamos where the sample was held in a reducing environment. The onset of strong dissipation at RUS frequencies starts at higher temperatures than it does at DMA frequencies and is different for the two types of resonance peaks. There is a small peak in Q^{-1} centred on ∼250 K, which appears to be associated exclusively with 'C_{44}'.

Variations of Q^{-1} are shown in figure 6. Below ∼400 K the lowest measurable value was ∼0.001, as determined by the spacing of 0.34 kHz between data points in the spectra. At larger Q^{-1} (higher temperatures) the peak widths were significantly greater than 0.34 kHz, and so were not

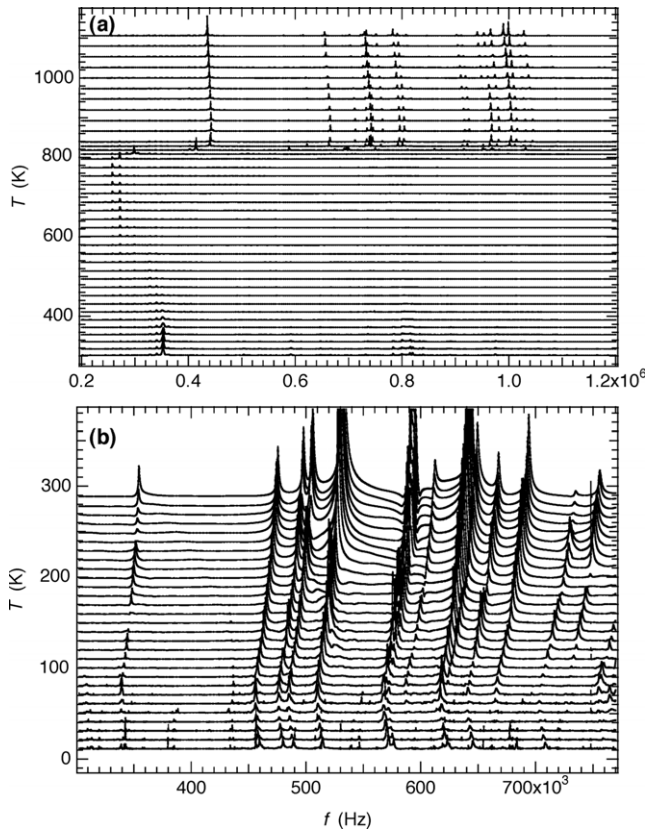

Figure 7. Stacks of RUS spectra from the ceramic sample of $LaAlO_3$. The y-axis is amplitude but the spectra have been displaced in proportion to the temperature at which they were collected and the axis is labelled as temperature. Resonance peaks are much weaker from the ceramic sample than from single crystals but they show the same pattern of variation with temperature. (a) At high temperatures the cubic $\leftrightarrow$ rhombohedral transition is marked by slight softening as $T \rightarrow T_c$ and then superattenuation at $T < T_c$. Weak peaks reappear below ~360 K. Low frequency peaks which do not vary with temperature are instrumental noise. (b) Below room temperature elastic softening is again evident as $T \rightarrow\sim 60$ K. At the lowest temperatures the spectra become relatively noisy.

constrained by spectral resolution. The values of Q^{-1} for 'C_{44}' and '$\frac{1}{2}(C_{11} - C_{12})$' obtained in this way are indistinguishable from data obtained from the Cambridge instrument in which crystals were heated in air (figure 6).

A second parallelepiped (1/2003) was heated and cooled in more or less the same way as the first had been in order to check the cubic $\leftrightarrow$ rhombohedral transition temperature, after rebuilding the high temperature RUS head. During cooling at 1 K min^{-1}, spectra collected down to 819 K contained sharp peaks. Spectra collected at 817 and 815 K did not contain resonance peaks. No further analysis was undertaken on these spectra. Both data sets are consistent with resonance peaks disappearing at 817 K.

3.4. Superattenuation and Q

Selection of peaks for the analysis of Q^{-1} for three different crystals, 1/2002, 2/2003 and 4/2002 (figure 6) was based on the output from the DRS software which showed which resonance peaks were providing information predominantly for '$\frac{1}{2}(C_{11} - C_{12})$' or '$C_{44}$', and on the requirement to have reasonably strong peaks without overlaps. Data for the $R\bar{3}c$ phase are in two groups, one determined by 'C_{44}' (67, 89, 92, 97 or 98%) and one by '$\frac{1}{2}(C_{11} - C_{12})$' (97% or 100%). Individual peaks selected from spectra for the cubic $Pm\bar{3}m$ phase depend predominantly on $\frac{1}{2}(C_{11} - C_{12})$ (98, 99%), C_{44} (98%) or K (65%). Data collected below room temperature are from a heating sequence, and data from the Los Alamos high temperature instrument are from a cooling sequence. The rest include a mix of data obtained from heating and cooling sequences. Q^{-1} in the stability field of the cubic phase was effectively constant for all the moduli and values fell in the range ~0.0001–0.0003. Even in the close vicinity of the transition temperature, there was no obvious increase in dissipation. The transition point itself appears to be marked by the sharp onset of complete attenuation of all acoustic resonances. Reverting to the opposite end of the temperature scale, the $R\bar{3}c$ phase has essentially the same anelastic properties as the $Pm\bar{3}m$ phase. In the intervening temperature interval, the variation of Q^{-1} shows a complex pattern, depending on temperature and frequency.

The onset of superattenuation was gradual with increasing temperature and was different for '$\frac{1}{2}(C_{11} - C_{12})$' and '$C_{44}$' (figure 6). Marked increases in Q^{-1} for 'C_{44}' started to develop at ~350 K, while for '$\frac{1}{2}(C_{11} - C_{12})$' the equivalent onset was at ~410 K. In the most favourable conditions (strong peaks, clean baseline), values of Q^{-1} up to ~0.02 can be resolved and these were reached by ~550 K for 'C_{44}'. The largest values of Q^{-1} resolved for '$\frac{1}{2}(C_{11} - C_{12})$' are in the vicinity of 0.012, at ~680 K. Apart from the higher values obtained at low temperature due to the low frequency resolution of the original spectra, data obtained for 1/2002 during cooling in a reducing atmosphere (Los Alamos) are indistinguishable from data obtained during heating or cooling in air (Cambridge). Although at the limit of resolution of the data, there appear to be two more or less reproducible breaks in slope near 430 and 510 K for the temperature dependence of 'C_{44}'. Equivalent breaks in slope are perhaps discernible near 520 and 600 K for Q^{-1} from '$\frac{1}{2}(C_{11} - C_{12})$'.

3.5. Ceramic samples

Spectra were collected from the first ceramic sample (cer1) in a heating sequence at ~10 K intervals from 302 to 527 K, at 1 K intervals from 784 to 834 K and in ~25 K steps from 839 to 1106 K (corrected temperature scale). Data collection at each temperature was preceded by an equilibration time of 10 or 15 min. In order to be sure of identifying all the resonance peaks of the sample in the stability field of the cubic phase, additional spectra were collected at high temperatures with the sample remounted so that it was held across a pair of edges and then across a pair of faces. Representative spectra are shown as a stack in figure 7(a). At room temperature the resonance peaks were weaker and broader than observed for a single crystal sample. They broadened and weakened with increasing temperature, until becoming undetectable above ~355 K. A single sharp peak which appeared to be due to the sample

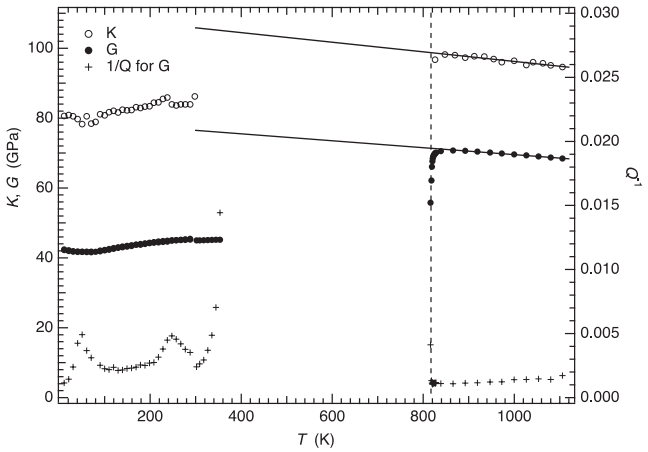

Figure 8. Variations of bulk modulus, K, shear modulus, G, and inverse mechanical quality factor, Q^{-1}, determined from RUS spectra for ceramic sample cer1. The temperature scale has been adjusted to give the $Pm\bar{3}m \leftrightarrow R\bar{3}c$ transition at 817 K (vertical dashed line). Straight lines through the data for the cubic phase have been extrapolated to below T_c so as to emphasize the extent of softening of both K and G due to the phase transition. Q^{-1} data are given for a resonance peak which occurs at ∼0.475 MHz at room temperature.

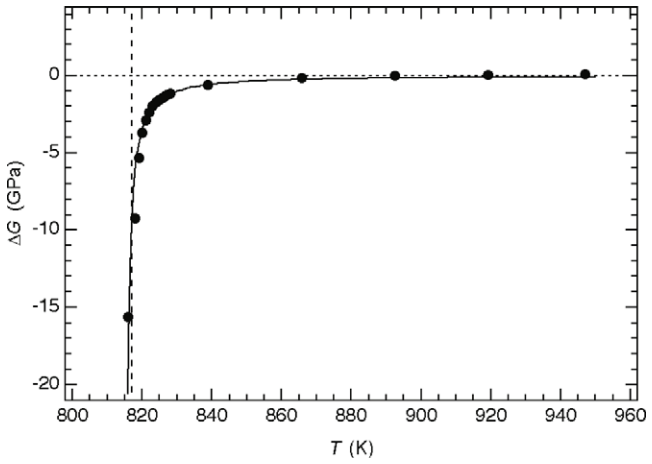

Figure 9. Pretransitional softening in cer1, as given by the difference between linear extrapolation of the data above 886 K (straight line in figure 8) and observed values of the shear modulus. The curve is a fit of equation (11) to the data using $T_c = 815$ K ($\kappa = -1.12$). The vertical dashed line is at 817 K.

was detected in the spectrum collected at 816 K, and spectra collected above this temperature contained numerous sharp peaks. There were no obvious differences between spectra collected at room temperature before and after heating.

Spectra were collected below room temperature in 30 K steps during cooling from 280 to 10 K and in 10 K steps during heating from 10 to 290 K. An equilibration time of 15 min was allowed before data collection at each temperature during cooling and 10 min during heating. Part of the stack of spectra collected in the heating sequence is shown in figure 7(b). The resolution of these spectra is better than obtained at high temperatures because the parallelepiped was sitting directly on the transducers. The spectra became relatively noisy at the lowest temperatures, however, probably due to resonances from components of the RUS head. The frequencies of all the peaks reduced slightly with increasing temperature from ∼10 to ∼70 K before increasing in a manner similar to the elastic stiffening observed for the single crystal parallelepipeds.

Values of K and G for polycrystalline $LaAlO_3$ in the stability field of the $Pm\bar{3}m$ structure were determined from the frequencies of ∼26–28 peaks measured in the high temperature spectra. Between 31 and 46 peaks were measured to obtain elastic modulus values for the $R\bar{3}c$ phase below room temperature. Rms errors of 0.6–0.8% signified relatively poor fits, with the greatest uncertainty being for K. Only a few peaks could be observed in spectra collected using the high temperature instrument when the sample was held in the stability field of the rhombohedral structure (see figure 7(a)), and it was not possible to determine values for G and K by fitting to peak frequencies. Instead, the frequencies of the strongest peak in the room temperature spectrum, at ∼0.35 MHz (corresponding to ∼100% G), and of the equivalent peak at ∼0.44 MHz in high temperature spectra were used to calibrate the relationship between peak frequency and G ($G = 0.2947 \times \text{frequency}^2$). This calibration was then used to determine values of G for temperatures between 10 and ∼355 K and for 816–825 K. The combined data are shown as a function of temperature in figure 8. In the stability field of the cubic phase K and G vary approximately linearly with temperature apart from in the range ∼816–850 K where some softening of G occurs ahead of the phase transition. Straight lines ($G = 79.47 - 0.0099T$, $K = 109.95 - 0.0137T$) have been fit to data in the range 886–1106 K in order to emphasize the substantial degree of softening shown by both K and G due to the $Pm\bar{3}m \leftrightarrow R\bar{3}c$ transition. The difference between this linear extrapolation and measured values at room temperature corresponds to a total softening of ∼20 and ∼26 GPa for K and G, respectively. The variation of G at low temperatures is similar to that of '$\frac{1}{2}(C_{11} - C_{12})$' and '$C_{44}$' in figure 4. K shows a slight softening with falling temperature, though the total change is probably less than the experimental uncertainty of the absolute values. Softening of G in the cubic stability field ahead of the phase transition was determined as the difference, ΔG, between observed values and the extrapolation of the straight line shown in figure 8. This softening is shown in figure 9.

Values of Q^{-1} determined from fitting of the lowest frequency peak (∼100% G) in all the spectra collected at high temperatures and to the peak at ∼0.47 MHz (∼88% G, 12% K) in the low temperature spectra have also been added to figure 8 (right hand axis). Absolute values of Q^{-1} determined from the ceramic data (∼0.001 for G of the cubic phase) are a factor of ∼10 larger than from single crystal data. An apparent increase at 816 K may be an artefact arising from imperfect fitting of a weak peak on an irregular baseline. The rhombohedral phase has Q^{-1} increasing from ∼0.001 at 10 K to ∼0.015 by ∼355 K. Two distinct peaks centred on ∼50 and ∼250 K are evident, each reaching a maximum value of ∼0.005 (analysed in detail in Carpenter *et al* (2009a)). There is then a steep increase starting just above room temperature, i.e. at slightly lower temperatures than the onset of superattenuation seen in the single crystal data and

more nearly at the temperature of onset of strong attenuation observed by Harrison and co-workers (Harrison and Redfern 2002, Harrison *et al* 2004b) (figure 6).

4. Discussion

Elastic softening at the $Pm\bar{3}m \leftrightarrow R\bar{3}c$ transition in $LaAlO_3$ has the general form expected for a second order transition in which octahedral tilting occurs on the timescale of strains induced by an applied stress, through strain/order parameter coupling. Data from the ceramic sample confirm the softening of both the shear and bulk modulus. This aspect of the elastic behaviour is dealt with quantitatively in Carpenter *et al* (2010b). Here attention is focused on dispersion with respect to frequency and stress for the elastic softening and anelastic dissipation behaviour.

Strong attenuation of acoustic resonances in RUS experiments has now been observed in association with cubic–tetragonal or cubic–rhombohedral phase transitions in perovskites with compositions $SrTiO_3$ (Migliori *et al* 1993), (Ca, Sr)TiO_3 (Walsh *et al* 2008), Sr(Zr, Ti)O_3 (McKnight *et al* 2009a, 2009b) and $LaAlO_3$ (Carpenter *et al* 2006, this study). The cubic phase typically has low Q^{-1} values (<0.001) and the transition to a tetragonal or rhombohedral structure is marked by an abrupt increase in Q^{-1} at a temperature which appears to correspond closely to the transition temperature. If there is any increase in dissipation ahead of the actual transition point, it appears to be restricted to a temperature interval of a few degrees at most. Dissipation in the tetragonal field of $SrTiO_3$ (Migliori *et al* 1993, McKnight *et al* 2009b) and in the rhombohedral stability field of $LaAlO_3$ (Carpenter *et al* 2006, this study) is sufficiently high that resonance peaks completely disappear from the RUS spectra. Resonance peaks also disappear from spectra obtained at high temperature from tetragonal phases in the (Ca, Sr)TiO_3 solid solution (Walsh *et al* 2008). In practice, the limiting value of Q^{-1} below which peaks can still be discerned is $\sim$0.02. For pure $SrZrO_3$ and members of the Sr(Zr, Ti)O_3 solid solution, the resonance peaks are broad but remain detectable in spectra from the tetragonal phase (McKnight *et al* 2009a, 2009b). The question then arises as to whether this dissipation is intrinsic and therefore understandable in terms of normal damping phenomena associated with phonon softening below a soft mode transition, or whether it is extrinsic and understandable in terms of anelastic domain wall motions under applied stress.

Factors which determine dissipation due to domain wall motion under an externally applied dynamic field can be understood at a phenomenological level using the equation of motion derived by Huang *et al* (1992) (e.g., Huang *et al* 1992, Wang and Huang 1994, Wang *et al* 1996, 2000, Chen *et al* 2000, Harrison *et al* 2004a). In its simplest form for ferroelastic twin walls being displaced through a distance x, this would be

$$M\ddot{x} + \Gamma\dot{x} + kx = F_C, \tag{1}$$

where F_C is the applied stress, M is an effective mass for the wall, Γ is the viscosity experienced by the moving wall and k is the restoring force. Dissipation is given in terms of a phase angle, δ, between the application of stress and the resulting strain as

$$\tan\delta = \Delta\frac{\omega\tau}{1+\omega^2\tau^2}. \tag{2}$$

In the case of a standard linear solid

$$\Delta = \frac{C_U - C_R}{C_R} \qquad (\text{for } (C_U - C_R) \ll C_R), \tag{3}$$

where C_U is the relevant elastic modulus for the unrelaxed state, excluding strain due to movement of the wall, and C_R the modulus of the relaxed state, including the strain due to movement of the wall to its new equilibrium position (Nowick and Berry 1972). The key external parameter is then the angular frequency, ω ($=2\pi f$), of the applied stress and the key response parameter is the relaxation time, τ, of the twin walls. In terms of the parameters in equation (1), the relaxation time is given simply by the ratio of the viscosity to the restoring force

$$\tau = \frac{\Gamma}{k}. \tag{4}$$

Huang *et al* (1992) included a force to represent interaction between adjacent domain walls, F_I, and Harrison *et al* (2004a) elaborated further by expressing restoring forces due to interaction between twin walls and the host lattice in terms of the wall energy as a function of position, $U(x)$, giving

$$M\ddot{x} + \frac{dU(x)}{dx} - F_I + \Gamma\dot{x} = F_C. \tag{5}$$

The restoring force, k, in equation (4) is then correspondingly more elaborate.

Dissipation processes can also be intrinsic, occurring as a consequence of interaction between strains induced by the applied stress and a more uniform property of the sample. For a phase transition driven by a soft optic mode this might be relaxation of the order parameter via its coupling with the strain. If there is bilinear coupling between the soft optic mode and a soft acoustic mode, critical slowing down of the order parameter as $T \rightarrow T_c$ according to the Landau–Khalatnikov mechanism can cause strong damping in a narrow temperature interval around T_c (Landau and Khalatnikov 1954, Rehwald 1973). The coupling in $LaAlO_3$ is not bilinear and there is no evidence for any such slowing down of acoustic phonons in the Brillouin spectra close to T_c, let alone over a temperature interval as wide as $\sim$450 K below T_c. Dissipation by relaxation of the central peak mode in response to an applied stress is a more realistic possibility. Using $\tau \approx 2 \times 10^{-8}$ s for the central peak mode, from Carpenter *et al* (2010b), requires $\omega \sim 5 \times 10^7$ for $\omega\tau = 1$ and hence $f \sim 10^7$ Hz. At lower temperatures, the central peak mode(s) might have longer relaxation times but 10^7 Hz is still a factor of $\sim$10 above most of the observed resonance frequencies of a $LaAlO_3$ parallelepiped with edge dimensions of $\sim$3–5 mm. Moreover, the central peak appears to couple with all the acoustic modes (see figure 9 of Carpenter *et al* 2010b) so that it would not be expected to give different coupling/relaxation behaviour for 'C_{44}' and '$\frac{1}{2}(C_{11} - C_{12})$'. The cause of superattenuation of acoustic resonances in $LaAlO_3$ at $\sim$1 MHz appears to be extrinsic, therefore, and relaxation of twin walls is currently

considered to be the most likely mechanism. The steep increase in Q^{-1} with increasing temperature has the same form as the steep increase in $\tan\delta$ ahead of the Debye peak seen in DMA experiments (figure 6), and could also depend on thermally activated depinning.

4.1. Dispersion of elastic softening with respect to frequency

In a dynamical mechanical analysis experiment using three-point bending geometry with a crystal plate that is long and thin, the Young's modulus parallel to the length is measured (Schranz *et al* 1999, Kityk *et al* 2000a, Harrison and Redfern 2002). For the first experiments of Harrison and Redfern (2002) and Harrison *et al* (2004c, 2004b), crystals were prepared with top and bottom surfaces parallel to (001) of the pseudocubic lattice, and the long axis parallel to [110]. The relevant Young's modulus for a static load would be $Y_{[110]}$, which is related to the moduli of a cubic crystal according to (following Nye 1985)

$$Y_{[110]} = \left(\frac{C_{11}}{2(C_{11} - C_{12})(C_{11} + 2C_{12})} + \frac{1}{4C_{44}} \right)^{-1}. \quad (6)$$

In this orientation, the applied load produces a resolved shear stress on the twin walls with an orientation which can induce them to move. For a separate experiment (Harrison *et al* 2004b) a crystal was prepared with top and bottom surfaces parallel to (001) and long axis parallel to [100]. The relevant Young's modulus for static loading is then

$$Y_{[100]} = \left(\frac{C_{11} + C_{12}}{(C_{11} - C_{12})(C_{11} + 2C_{12})} \right)^{-1}. \quad (7)$$

In this orientation any resolved stresses on the twin walls should not be at an angle which would cause them to move. Under dynamic loading, elastic and anelastic behaviour is characterized by two properties, the storage modulus and the energy loss per cycle (dissipation). The storage modulus is the real component of the Young's modulus, e.g.

$$Y'_{[110]} = |Y_{[110]}| \cos\delta \quad (8)$$

and the dissipation is $\tan\delta$. Values of $\tan\delta$ obtained at room temperature by Harrison and co-workers were generally small, so that the measured value of Y' is close to the static loading value, Y.

Complete calibration of the elastic moduli (this study and Carpenter *et al* 2010b) allows absolute values for the Young's modulus to be calculated for the cubic phase and estimated for the twinned rhombohedral phase at room temperature. Taking $C_{11} = 317$, $C_{12} = 131$ and $C_{44} = 157$ GPa for the cubic phase (table 3 of Carpenter *et al* 2010b) gives $Y_{[100]} = 240$ and $Y_{[110]} = 326$ GPa. Taking the values of C_{44} and $\frac{1}{2}(C_{11} - C_{12})$ from cubic fits of room temperature RUS spectra, together with the room temperature bulk modulus from Brillouin scattering, gives average values of $C_{11} = 276$, $C_{12} = 156$, $C_{44} = 146$ GPa, and $Y_{[100]} = 163$, $Y_{[110]} = 273$ GPa as estimates for twinned crystals at room temperature. Observed values of $Y_{[100]}$ from figure 15 of Harrison *et al* (2004b) are 175 and 120 GPa, corresponding to ~73% and ~74%, respectively, of the calculated values. According to Schranz *et al* (1999) and Kityk *et al* (2000a) the accuracy of moduli measured by DMA is not expected to be better than 20% but relative accuracy should be ~0.2–1%. On this basis, agreement is satisfactory for absolute values of $Y_{[100]}$ and good for the difference between cubic and rhombohedral phases. The form of the underlying elastic softening, excluding the influence of the additional twins (figure 15 of Harrison *et al* 2004b), had a distinct curvature very similar in form to that observed for the intrinsic elastic moduli by Brillouin spectroscopy (Carpenter *et al* 2010b). The purely elastic part of this softening due to the phase transition thus appears to have been essentially the same at ~1 Hz and at ~10^{10}–10^{11} Hz.

Values of $Y_{[110]}$ estimated from data given in figure 6 of Harrison and Redfern (2002) are 94 GPa for the cubic phase and 50 GPa for the rhombohedral phase at room temperature, corresponding to 29% and 18% of the observed values. The absolute error is much larger, but of greater concern is the difference in scaling for the cubic and rhombohedral phases. (Observed room temperature values actually varied between 90 and 140 GPa (at low $\tan\delta$) for differing loading and measurement frequencies; see figure 3 of Harrison *et al* 2004c.) Failure of the calculation to reproduce a relative scale for the DMA data for [110] crystals could be due to sample geometry. The plate cut for measurements of $Y_{[100]}$ was half as thick (0.25 mm) as the plates used for $Y_{[110]}$ (0.52 mm) and it is therefore possible that the former more nearly approached the length: thickness ratio required to effectively exclude the influence of the shear modulus (cf equation (2) in Kityk *et al* 2000a). If this explanation is the correct, it follows that measurements on [110] plates would all have depended on the much softer shear modulus in addition to the [110] Young's modulus. Some of the elastic softening and twin wall motions observed by Harrison and Redfern (2002) and Harrison *et al* (2004c, 2004b) would then have been related to shear stresses rather than, more simply, to compressive/extensional stresses parallel to the length of each crystal.

As shown in figure 6 of Carpenter *et al* (2010b), results for the shear elastic moduli $\frac{1}{2}(C_{11} - C_{12})$ and C_{44} measured in the stability field of the cubic phase by RUS and Brillouin spectroscopy are indistinguishable, even to the extent of showing the same slight softening as $T \rightarrow T_c$ from above. There appears to be no intrinsic dispersion measurable between ~10^5 and ~10^{10} Hz therefore. The Brillouin value of the bulk modulus is ~0.5% smaller than the RUS value at ~1000 K, but this is well within experimental uncertainty. In the stability field of the rhombohedral phase, the average values of C_{44} measured by RUS are close to the values obtained by Brillouin scattering. As C_{44} should be the same for all twins in the RUS sample, this is again consistent with there being little or no dispersion. Values of $\frac{1}{2}(C_{11} - C_{12})$ in the RUS measurements represent some average for the different twin orientations and would not necessarily be the same as the Brillouin values, as is also observed (figure 6 of Carpenter *et al* 2010b). More significantly, the Brillouin and RUS values of $\frac{1}{2}(C_{11} - C_{12})$ show the same non-linear dependence on temperature as $T \rightarrow T_c$ from below. In other words, the RUS measurements outside

the superattenuation regime determine essentially the same elastic softening as found from velocities of acoustic phonons within individual twins.

The non-linear temperature dependence of individual moduli for the rhombohedral phase of $LaAlO_3$, particularly at temperatures above ~700 K, was explained qualitatively by Carpenter *et al* (2010b) as being due to coupling between acoustic modes and a central peak mode. The relaxation time associated with the central peak mode was estimated to be ~10–100 ps, which is certainly short enough to allow complete relaxation on the timescale of elastic resonances in an RUS experiment. Similar non-linear softening is evident in the DMA results of Harrison *et al* (2004b) for $Y_{[100]}$, which is independent of C_{44} (equation (7)). It appears that $\frac{1}{2}(C_{11}-C_{12})$, at least, is the same when measured at ~1, ~10^5 and ~10^{10} Hz, and includes the influence on the acoustic modes of coupling with the central peak mode(s).

4.2. Dispersion of dissipation with respect to frequency and stress

Harrison and co-workers (Harrison and Redfern 2002, Harrison *et al* 2004c, 2004b) measured the real and imaginary components of the Young's modulus of single crystal $LaAlO_3$ by dynamical mechanical analysis with three-point bending geometry. They used frequencies of 0.1–50 Hz and applied different static and dynamic loads from room temperature up to ~870 K. Their crystals were also supplied by Crystal GmbH, Berlin, and are therefore likely to have had the same physical and chemical characteristics as the samples used in the present study. A characteristic pattern of elastic and anelastic anomalies was attributed predominantly to the back and forth motion of the tips of needle twins under dynamic loading (Harrison and Redfern 2002, Harrison *et al* 2004c, 2004b). In the stability field of the cubic phase the crystals had nearly constant values of the storage modulus and low values of $\tan\delta$ ($\tan\delta \approx 0.02$–0.04). The cubic $\leftrightarrow$ rhombohedral transition was marked by a steep drop of the storage modulus and a concomitant increase in $\tan\delta$. Between ~750 and ~470 K, an interval of extreme (superelastic) softening was observed, with the elastic modulus reduced to about 10% of its value in the stability field of the cubic phase. This was attributed to the high mobility of twin walls, as proposed also by Schranz *et al* (Schranz *et al* 1999) and Kityk *et al* (2000a, 2000b) for $SrTiO_3$. Below ~470 K an increase in elastic modulus was accompanied by a maximum in the mechanical loss, attributed to immobilization of the twin walls by the pinning influence of defects. Below the freezing interval, both the elastic modulus and $\tan\delta$ returned to values comparable to those of the cubic phase. Activation energies in the range ~85–95 kJ mol^{-1} associated with the freezing process were interpreted as indicating that the defects responsible for pinning were oxygen vacancies.

Data for $\tan\delta$ from figure 2 of Harrison *et al* (2004c) have been added to figure 6 to allow direct comparison between the typical behaviour observed by DMA at ~10^{-1}–10^2 Hz and by RUS at ~10^5–10^6 Hz. Although both experiments reveal a steep increase in dissipation with increasing temperature, consistent with a common, twin wall related origin for the anelastic behaviour, there are two observations which suggest that the mechanisms being sampled could be different in detail. Firstly the values of $\tan\delta$ reported by Harrison and Redfern (2002) are at least an order of magnitude greater than Q^{-1} from RUS. When Q^{-1} is determined by the resonance peak width at half height method, as in the present study, it is related to $\tan\delta$ according to Lee *et al* (2000) and Lakes (2004) as (for small damping)

$$\tan\delta \approx \frac{1}{\sqrt{3}}\frac{\Delta f}{f} = \frac{1}{\sqrt{3}}Q^{-1}. \tag{9}$$

Values of Q^{-1} obtained using RUS Walsh *et al* (2008) are lower by a factor of 10 than values obtained for $\tan\delta$ by DMA (Harrison *et al* 2003) from rather similar ceramic samples of (Ca, Sr)TiO_3 in the stability field of the cubic structure, and by a factor of ~100 for single crystal $LaAlO_3$ in the cubic field (compare this study with Harrison and Redfern 2002). Some of the difference in absolute values of $\tan\delta$ and Q^{-1} could be due to instrumental factors, but the anelastic contributions to elastic properties of the rhombohedral phase measured at RUS frequencies are generally on a substantially smaller scale than the effects observed by DMA.

The second important difference relates to the level of stress required to initiate the movement of needle twins. Harrison and Redfern (2002) found that it was necessary to apply stresses in excess of some critical value before superelastic behaviour was induced. The effective stress experienced by the sample in an RUS experiment is not known, but it is possible to compare the strains involved. From figure 11 of Harrison and Redfern (2002), loading to produce a displacement of at least ~2.5×10^{-4} mm at the midpoint of a crystal supported by knife edges 5 mm apart occurred prior to the onset of the superelastic regime. This corresponds to a shear strain of ~$(2.5 \times 10^{-4})/2.5 = 10^{-4}$. Harrison *et al* (2004c) obtained force versus displacement curves which were broadly the same as for the first [110] crystal but with some differences (compare figure 8 of Harrison *et al* 2004c, with figure 11 of Harrison and Redfern 2002). In particular, curvature in the superelastic regime was reversed and breaks in slope interpreted previously as the onset of superelastic behaviour were not clearly defined. By extrapolation to lower loads, the changes in slope might have occurred at a displacement of ~10^{-5} mm, say, giving a shear strain of ~$(10^{-5})/2.5 \approx 10^{-6}$. Surface displacements of a resonating parallelepiped have been observed by laser-Doppler interferometry to be ~1 nm (Ogi *et al* 2004) and, as discussed by Walsh *et al* (2008), imply effective strains of up to ~10^{-7}. Such strains do not equate directly to the resolved shear stress experienced at a given twin wall but the difference suggests that the effective stresses could be an order of magnitude smaller in the RUS experiment. The expectation, therefore, is that the critical stress described by Harrison and Redfern (2002) as being required to initiate wholesale twin wall mobility would not be achieved in a resonating parallelepiped.

An entirely separate indication that superattenuation observed in the RUS experiments is not due to the same movement of needle twins as in the DMA experiments is provided by extrapolation of measured Arrhenius relationships

to high frequencies. Harrison and Redfern (2002) and Harrison *et al* (2004c) described twin wall motion in the temperature interval of domain wall freezing as a thermally activated process such that the relaxation time has a strong temperature dependence according to

$$\tau = \tau_o \exp\left(\frac{E}{RT}\right), \qquad (10)$$

where τ_o is constant, E is the activation energy, R is the gas constant and T is temperature. Data from figure 5 of Harrison *et al* (2004c) for the frequency of the peak in $\tan\delta$ as a function of temperature for the lowest static load are reproduced here in figure 10. These represent temperatures at which $\omega\tau = 1$ and define a straight line with $E = 94$ kJ mol^{-1}. Temperature limits for the freezing interval have then been estimated using the approximate limits of the peak in $\tan\delta$ and breaks in curvature of the elastic modulus data given in figure 3 of Harrison *et al* (2004c), again for the lowest load. These limits are shown in figure 10, and their extrapolation to high frequencies using the same value of E suggests that needle twins should be immobile below ~650 K at ~0.4 MHz. This is well above the onset temperature of ~350 K for strong attenuation of resonance peaks in the RUS spectra. Accordingly, even if the real stress on twin walls in an RUS experiment exceeds the critical stress required to initiate wholesale needle tip motion, there should be insufficient thermal energy for this mechanism to operate below ~650 K.

The possibility of needle tip motion at low stress and high frequencies is not totally precluded by the data, however. In figure 10 the same value of $E = 94$ kJ mol^{-1} has been used to extrapolate the onset of RUS attenuation to low temperatures, as if the same microscopic pinning mechanism is involved. At 1 Hz this additional attenuation might develop at temperatures above ~250 K while at room temperature it would become observable at frequencies of less than ~2 kHz. Harrison *et al* (2004c) observed significant anelastic softening (low storage modulus and $\tan\delta \geqslant 0.2$) at room temperature for loading frequencies of $<\sim 1$ Hz. This behaviour occurs well below the main freezing interval and was attributed to displacements of weakly pinned needle tips. If some weakly pinned needle tips can move without the requirement of applying a critical stress, their motion should be detectable in both RUS and DMA experiments. On the other hand, the contribution of needle tip motion to the DMA results may simply be obscuring much smaller contributions from a separate mechanism implied by the extrapolation of the RUS attenuation limit.

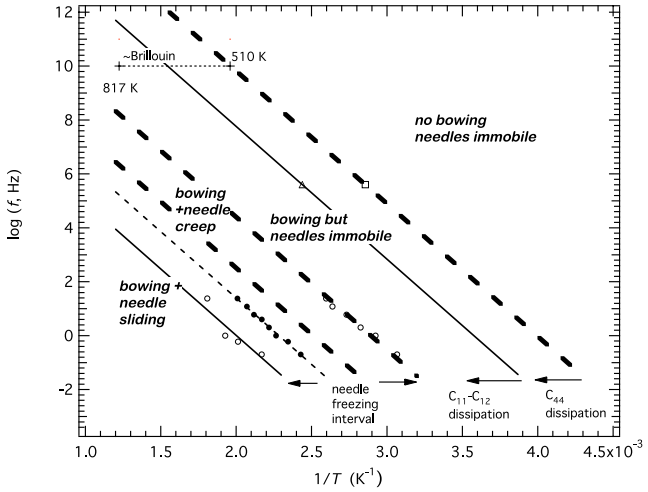

Figure 10. Anelasticity map for different dissipation mechanisms as a function of temperature and frequency. Filled circles represent the peak temperatures for $\tan\delta$ at low frequencies (at the lowest applied stress) reproduced from figure 5 of Harrison *et al* (2004c). The straight, dashed line fit to these data gives an activation energy of 94 kJ mol^{-1}. Open circles represent limits of the twin wall freezing interval as estimated from changes in slope of $\tan\delta$ and the storage modulus as a function of temperature in figure 3 of Harrison *et al* (2004c). Straight lines through these have been constrained to have the same slope as for the peak in $\tan\delta$. Straight lines, also with the same slope, are shown passing through data points for the estimated onset of dissipation associated with '$\frac{1}{2}(C_{11} - C_{12})$' (open triangle) and '$C_{44}$' (open square) at ~0.4 MHz in RUS spectra. Thick broken lines then define fields in which different dissipation mechanisms might operate. The boundary between creep and sliding for needle domains has been taken as 433 K, 10 Hz from data given in figure 6(a) of Harrison *et al* (2004c) with the same slope as for the peak in $\tan\delta$. Extrapolation of the RUS limits to high frequencies would imply that the proposed bowing mechanism of domain wall motion could operate at Brillouin frequencies. A dashed line showing this possibility between ~510 and 817 K is shown at 10^{10} Hz for illustration.

4.3. Alternative mechanisms for twin wall motion

Figure 11 shows a cartoon of possible transformation twin wall responses when a shear stress, σ, is applied to a crystal in an orientation which is appropriate to cause wall movement. If the deformation is of a single twin domain (figure 11(a)) the resulting strain, e, is given by $e = s_{\text{crystal}}\sigma$, where s_{crystal} is the relevant single crystal compliance. If the walls move, an additional strain is released so that the total strain is given by $e = (s_{\text{crystal}} + s_{\text{walls}})\sigma$. The contribution of the twin walls, s_{walls}, to the total compliance depends on an effective spring constant related to the restoring force on the wall, the volume of crystal converted from one twin orientation to another and the magnitude of the symmetry breaking spontaneous strain (Schranz *et al* 1999, Kityk *et al* 2000a, 2000b, Carpenter 2007). In practice, changes in twin orientation can occur by a lateral movement of the twin walls, which might also involve a degree of tilting out of their normal crystallographic plane (1 in figure 11(b); and see figure 10 of Kityk *et al* 2000a, or figure 12 of Harrison and Redfern 2002), advance or retraction of a needle tip (2 in figure 11(b); and see Harrison *et al* 2004c, 2004b, 2004a) or local bowing (3). In a dynamic loading experiment, dissipation arises as a consequence of the effective viscosity experienced by moving twin walls, due to extrinsic effects, such as interaction with defects, and intrinsic effects, such as interaction with phonons. On the basis of direct comparison with results from DMA experiments discussed above, movement of needle tips is not considered to be the likely mechanism under the high frequency, low stress conditions of RUS. Displacement or tilting of the twin walls along their full length is unlikely since this requires a high degree of correlation over a length scale of millimetres on a timescale of microseconds. As a working hypothesis,

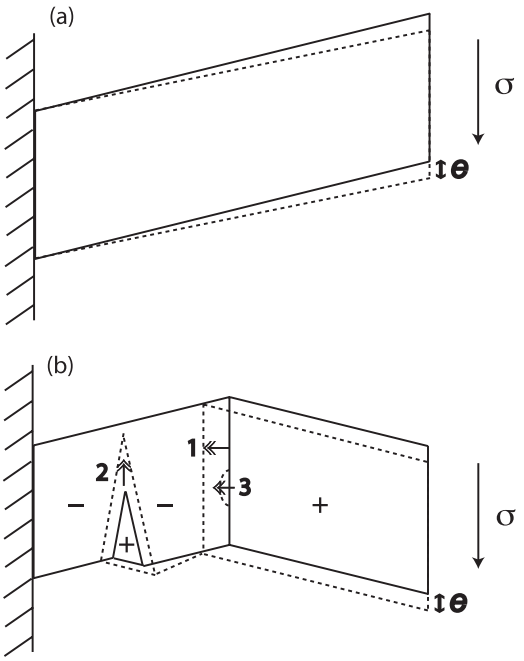

Figure 11. Cartoons illustrating possible twin wall displacements under the influence of an externally applied stress. (a) A shear stress, σ, applied to a crystal which does not contain twins will cause a strain, e, dependent on the intrinsic elastic compliance of the crystal. (b) If the same stress is applied to a crystal containing transformation twins, the resolved stress on the twin walls may cause them to move. A twin wall might be displaced laterally (1), with or without some tilting out of its preferred crystallographic plane, and a needle twin might grow by advancement of the tip (2). Finally, the walls may experience bowing (3) at some local length scale. For case (a) the total strain will be greater than for (b) and will depend both on the intrinsic compliance of the crystal and the effective compliance of the twin walls.

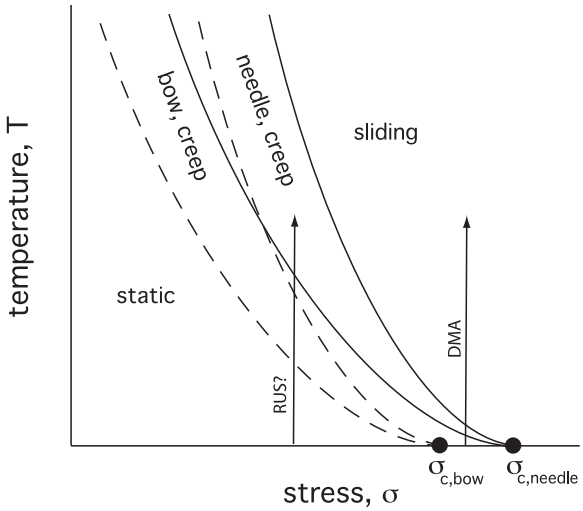

Figure 12. Schematic anelasticity map for different dissipation mechanisms as a function of temperature and stress (following Natterman *et al* (2001)). A critical stress, σ_c, is shown at 0 K to represent the magnitude of stress which would be required to release a twin wall from pinning points due to interaction with defects. At high temperatures, pinning behaviour leads to three regimes—static walls, creep and domain wall sliding. If there are two (or more) mechanisms by which the domain walls can move and these have different critical stresses for release from pinning points, there will be additional fields of anelastic dissipation. Separate static, creep and sliding fields are shown here for needle domain and local bowing motions. Differences in the dissipation behaviour of $LaAlO_3$ can then be understood in terms of different levels of applied stress involved. A trajectory of increasing temperature is shown at relatively low stress for an RUS experiment and at relatively high stress for a DMA experiment.

therefore, it is proposed that the key dissipation mechanisms arise from interactions of bowed sections of the twin walls with defects and phonons.

The literature on domain wall motion in ferromagnetic, ferroelectric, piezoelectric and ferroelastic materials is substantial, but the phenomenological model of Natterman *et al* (2001) is, in principle, quite general and provides insights into domain wall dynamics in both ferromagnetic (Chen *et al* 2002) and ferroelastic materials (Harrison *et al* 2004b, 2004a). When domain walls can be weakly pinned by defects, there are expected to be three possible regimes of mobility in temperature–frequency–stress space (not considering the field of saturation at large strains). For stresses below the critical threshold required for unpinning, there is no macroscopic motion of the walls but there can still be relaxations of local segments between metastable positions (static regime). If temperature and/or stress are increased, sufficient energy becomes available for segments of the walls to escape from their pinning positions and a thermally activated creep motion is expected (creep regime). At sufficiently high temperatures and levels of stress, the domain walls become effectively free to sweep across the sample (domain wall sliding regime). The expected pattern for these regimes as a function of temperature and stress is reproduced after Natterman *et al* (2001) in figure 12. The same fields must appear in the frequency domain, such that for a given stress at a given temperature, reducing frequency produces transitions from static walls, through creep to the sliding regime (figure 10). In combination, figures 10 and 12 then constitute anelasticity maps analogous to Ashby deformation mechanism maps for plastic deformation (Ashby 1972).

If there are two separate mechanisms of wall motion which have different critical stresses for initiation of their escape from pinning points, two sets of mobility regimes should appear in the anelasticity maps. Different regimes are suggested in figure 12 for needle tip displacement and bowing, and the resulting topologies can be used to assess expected behaviour for different stress/frequency/temperature trajectories. The boundary between static and creep regimes for both bowing and needle tip motion in figure 10 is assumed to be delineated by the temperature, for a given frequency, at which there is a steep increase in dissipation. The boundary between creep and sliding regimes for needle domains has been estimated from the data of Harrison *et al* (2004b) who identified the transition using Cole–Cole plots. From their figure 6, the transition at 160 °C occurs at ∼10 Hz (100 mN static load). This corresponds closely to a point on the tan δ curve for 12 Hz in their figure 3 where there is a break in slope below the Debye peak. This point has been added to figure 10 and a

straight line for $E = 94$ kJ mol^{-1} drawn through it for the upper temperature limit of needle domain creep.

There are no quantitative results for the stress/temperature domain and so critical stresses for depinning of needle tips and bowed segments of domain wall at 0 K are shown schematically in figure 11 as $\sigma_{c,needle}$ and $\sigma_{c,bow}$ respectively. The resolved stress on the twin walls for a given DMA experiment has been placed between these and the stress in an RUS experiment is shown as being less than $\sigma_{c,bow}$. On this basis, increasing temperature in an RUS experiment should give a sequence static $\rightarrow$ creep $\rightarrow$ sliding regimes for bowing and might reach the creep regime for needle tips. The DMA experiment shown as an example (at constant frequency) would give bowing in the sliding regime, even at the lowest temperature, followed by needle creep and needle sliding. The argument for distinguishing mechanisms in this way comes down to the difference between $\sigma_{c,needle}$ and $\sigma_{c,bow}$. For advance or retraction of a needle domain, it is necessary to unpin both the tip itself and lengths of two walls on either side of the tip, but for a bowing movement it is only necessary to unpin a segment of the wall. The critical stress for unpinning a segment of wall is a complex function of the length, L, of the segment, however, and depends on the Larkin length, L_p (Natterman *et al* 2001, Mueller *et al* 2002). L_p is the smallest length scale over which the wall can be roughened and pinned due to balancing of the elastic energy associated with introducing curvature relative to the strength of interaction with defects (together with their concentration). The value of $\sigma_{c,bow}$ in turn depends on L_p^{-2} (Lyuksyutov *et al* 1999, Glatz *et al* 2003). A quantitative evaluation is not yet possible for $LaAlO_3$ because values for the relevant parameters are not known.

Contrasting anelastic behaviour for the two mechanisms depends on the parameters given in equations (1)–(5). Various interpretations can be placed on the physical meaning of these parameters, but a simple view is that forces which act to oppose needle tip motion within a crystal arise predominantly from interactions with defects $U(x)$, wall–wall interactions (F_I) and viscous drag (Γ) from disruption of phonons behind the moving wall (Combs and Yip 1983, Huang *et al* 1992, Wang *et al* 1996, Harrison *et al* 2004a). For bowing of a ferroelastic twin wall, the same forces apply but $U(x)$ will contain an additional restoring force due to the fact that the twin plane in the bowed region becomes tilted out of its normal low energy crystallographic plane (Salje and Ishibashi 1996, Harrison and Redfern 2002). A larger restoring force (k in equation (1)), corresponding to a smaller compliance for the wall (s_{walls}), will give smaller values of τ and smaller displacements. Both anelastic softening and dissipation are then expected also to be correspondingly smaller. According to these qualitative arguments, an RUS experiment should provide evidence only of relatively small anelastic relaxations from small domain wall displacements. In a DMA experiment, contributions from the bowing mechanism would generally be hidden by the much larger contributions of mobile needle domains.

In the proposed model, the increasing dissipation observed for 'C_{44}'-related resonance peaks of $LaAlO_3$ above ~350 K is due to interaction between twin walls and defects at the start of the creep regime of twin wall bowing. The relaxation time and, hence, Q^{-1} should be determined by the activation energy for unpinning. If the sliding regime is reached at higher temperatures, dissipation will depend on the viscosity, Γ. Only stresses which induce the shear strain e_4 (with respect to a cubic reference system) should cause transformation twin walls in rhombohedral crystals to move, however, and it is necessary to consider the behaviour of '$\frac{1}{2}(C_{11} - C_{12})$' peaks separately. Q^{-1} from the small 'C_{44}' component would contribute to their attenuation, but a more likely cause is the off-diagonal terms such as C_{14}, C_{24}, etc, in the elastic modulus matrix, which take non-zero values in the stability field of the rhombohedral structure (Carpenter *et al* 2010b) and link e_4 strains to stresses such as σ_1 and σ_2. On the other hand, the temperature at which there is a steep increase in Q^{-1} for '$\frac{1}{2}(C_{11} - C_{12})$' resonance peaks, i.e. ~600 K (figure 6) coincides with the temperature at which the onset for creep of needle twins passes through ~0.4 MHz (figure 9). If this is not simply fortuitous, it could imply that the steep increase in dissipation is related to the mobility of needle tips. For the ceramic sample, all the peaks depend predominantly on the shear modulus which, in turn depends on both 'C_{44}' and '$\frac{1}{2}(C_{11} - C_{12})$', and the increase in Q^{-1} above ~350 K presumably depends predominantly on Q^{-1} for 'C_{44}'.

The RUS data show additional unexplained details, such as possible breaks in slope for Q^{-1} as a function of temperature from both types of resonance peaks. These hint at the possibility that the superattenuation interval contains overlapping peaks, as is found, for example, in the mechanical dissipation behaviour of PZT (Wang *et al* 2001) and DKDP (Huang *et al* 1997). It is also worth noting that oxygen vacancies are known to play a role in the pinning of needle domain tips at low frequencies of applied stress, but that any difference in the concentration of oxygen vacancies between reducing (Los Alamos) and oxidizing (Cambridge) conditions in the present study is not sufficient to change the dissipation behaviour at RUS frequencies and stresses. The use of more severely reducing or oxidizing conditions could provide a separate test of the role of oxygen vacancies in the twin wall pinning processes.

4.4. Extrapolation to high temperatures and phonon frequencies

Extrapolation of the onset of C_{44} attenuation from RUS frequencies to phonon frequencies, using a slope determined by $E = 94$ kJ mol^{-1}, gives an onset temperature of ~510 K at 10^{10} Hz, ~570 K at 10^{11} Hz and ~650 K at 10^{12} Hz (figure 10). Implicit in such an extrapolation is the assumption that the dissipation is due to thermally activated domain wall mobility is constrained by the same pinning mechanism as occurs at lower temperatures and lower frequencies. The twin walls themselves may not be quite the same, however. At low temperatures, they do not occupy a significant volume fraction of a crystal because they are thin and their spacing is wide in comparison with their thickness. The width, w, and density, N, of twin walls are expected to increase as $T \rightarrow T_c$ according to $w \propto N \propto (T_c - T)^{-1}$ for a second order transition (Wenyuan *et al* 1985, Yening *et al* 1987, Salje 1990, Chrosch and Salje

1999). Chrosch and Salje (1999) obtained $w \approx 50$ Å at 600 K and ≈200 Å at 800 K for $LaAlO_3$. Also as $T \rightarrow T_c$ the strain contrast between twin domains diminishes and the distinction between domain walls and the domains themselves becomes progressively more diffuse. Thick walls are less likely to be pinned by defects than thin walls (Lee *et al* 2006) and once they become mobile the resulting structural variations could more appropriately be discussed in terms of dynamic fluctuations of the order parameter on the length scale of the expected wall thicknesses. The central peak intensity also varies approximately as $(T_c - T)^{-1}$ (figure 14(c) of Carpenter *et al* 2010b), but it does not necessarily follow that there is a causal relationship between changes in twin wall properties and phonon density fluctuations discussed in relation to the quasi-elastic scattering observed by Brillouin spectroscopy. The correlation perhaps arises only because the central peak behaviour is related to the order parameter susceptibility, which is also expected to scale as $(T_c - T)^{-1}$. The central peak disappears close to $T = T_c$ (Carpenter *et al* 2010b) and the attenuation of acoustic resonances also drops abruptly at T_c (this study).

Optical observations of twin wall distributions in mm sized single crystals of $LaAlO_3$ have not given a precise temperature at which the walls might become mobile but indicate, at least, that gross changes in microstructure observed as $T \rightarrow T_c$ might start to occur above ∼730 K (Hayward *et al* 2005, Carpenter *et al* 2010b). This correlates with a break in slope of (frequency)^2 versus T for the E_g soft optic mode (Hayward *et al* 2005). The wavenumber of the E_g mode at this point is 10 cm^{-1}, corresponding to a frequency of $\sim 10^{11}$ Hz. The point $f = 10^{11}$ Hz, $T = 730$ K falls within the field of twin wall bowing shown in figure 10, but does not obviously match up with the extrapolated boundary for the onset of this loss mechanism. Hayward *et al* (2005) associated the wall unpinning mechanism with increasing mobility of the pinning defects (rather than with increased thermal energy of walls in a static field), and speculated that 730 K marks a change from static clustering to dynamical disorder of the oxygen vacancies. Whatever the precise unpinning mechanism might be, domain wall mobility clearly can be implicated in the anomalous structural evolution of rhombohedral $LaAlO_3$ at high temperatures.

4.5. Elastic softening in the stability field of the cubic phase

Elastic softening as a second order displacive transition point is approached from above can be described effectively with an expression of the form

$$\Delta C_{ik} = A_{ik}(T - T_c)^{\kappa}, \tag{11}$$

where ΔC_{ik} are deviations of a single crystal moduli from their trends in the high symmetry phase, and κ, A_{ik} are material constants. The underlying mechanism has been interpreted in terms of fluctuations due to interactions between modes with k-vectors just away from the critical point of the Brillouin zone (Höchli 1972, Cummins 1979, Lüthi and Rehwald 1981, Yao *et al* 1981, Fossum 1985, Carpenter and Salje 1998, Carpenter 2007). In the case of a cubic parent phase the constraints of symmetry allow softening only of C_{11} and C_{12} due to this mechanism, with $\Delta C_{11} = \Delta C_{12}$. Accordingly, the bulk modulus, $K = \frac{1}{3}(C_{11} + 2C_{12})$ is expected to soften while $\frac{1}{2}(C_{11} - C_{12})$ is not. In reality K, $\frac{1}{2}(C_{11} - C_{12})$ and C_{44} all soften (figure 5) and equation (11) provides a convenient empirical description which can be used to compare their softening. Using $T_c = 817$ K, a value of $\kappa = -1.10$ is obtained for ΔC_{44}. The fit is improved using $T_c = 815$ K, with $\kappa = -1.32$, $A = -66.1$ GPa. A similarly good fit is obtained for $\Delta(\frac{1}{2}(C_{11} - C_{12}))$ with $T_c = 815$ K, $\kappa = -1.09$, $A = -32.4$ GPa (figure 5). Fits to the data for ΔK are relatively poor if $T_c = 815$ K ($\kappa = -0.73$) is used, however, and a substantial improvement is obtained using $T_c = 797$ K ($\kappa = -1.96$, $A = -1514$ GPa) (figure 5). The fit shown for ΔG in figure 9 was constrained to $T_c = 815$ K, giving $\kappa = -1.12$, $A = -21.4$ GPa, and is thus consistent with the single crystal shear elastic moduli. A high degree of correlation between the fit parameters and sensitivity also to the choice of baseline means that it is safe only to conclude that softening of the bulk modulus is different from that of the symmetry-adapted shear elastic moduli, and that values of κ are in the range ~ -1–1.3 for the latter. There is also the suggestion that the transition temperature for symmetry breaking is a few degrees below 817 K, and that the complex evolution of elastic moduli observed by Brillouin spectroscopy in the interval ∼797–817 K could be related to two separate instabilities.

There is a clear correlation of all the pretransitional softening with the tails of volume strain, $3e_1$, and excess heat capacity into the stability field of the cubic phase (figures 1(b) and 2, respectively, of Carpenter *et al* 2010b). A further correlation exists between the onset of these pretransitional effects, the break in slope of electrical impedance at ∼890 K shown in figure 13(b) of Hayward *et al* (2005) and the development of quasi-elastic scattering below ∼860 K in inelastic neutron scattering experiments (Axe *et al* 1969). Axe *et al* (1969) attributed the quasi-elastic scattering to overdamping of the soft mode.

In $KMnF_3$ softening of C_{12} extends to ∼70 K above T_c with $\kappa \approx -1.4$ for ΔC_{12} (data of Cao and Barsch 1988, analysed in Carpenter and Salje 1998). Salje and Zhang (2009) obtained κ values in the range 0.4–0.8 for $KMn_{1-x}Ca_xF_3$ ($x = 0$–0.023) single crystals with long axes parallel to [100] by DMA. In this orientation the measured elastic modulus includes contributions from both $(C_{11} - C_{12})$ and $(C_{11} + 2C_{12})$ (equation (7)). In $SrTiO_3$ the softening interval is similar and Carpenter (2007) obtained $\kappa \approx -1.2$ for ΔC_{11} and ΔC_{12}. The value of κ for zone-centre combinations of elastic moduli is expected to vary between $-1/2$ and -2, depending on the anisotropy and dispersion of soft branches around the critical point (Axe and Shirane 1970, Pytte 1970, 1971, Höchli 1972, Carpenter and Salje 1998). For a system with softening along only one branch of the soft mode, $\kappa \approx -3/2$ is predicted, while softening in three dimensions is expected to give $\kappa \approx -1/2$. Inelastic neutron scattering results for $LaAlO_3$ show that there is some softening away from the R point of the Brillouin zone in at least two dimensions (Axe *et al* 1969, Kjems *et al* 1973), but to a much lesser extent than occurs between the R and M

points in $KMnF_3$ and $SrTiO_3$ (Gesi *et al* 1972, Kjems *et al* 1973). Without a definitive value for T_c, the data for ΔK of $LaAlO_3$ are ambiguous; using the fit from $T_c = 815$ K would imply softening in three dimensions while the fit using $T_c = 797$ K would imply softening along only one direction.

5. Conclusion

In combination, the present series of papers on $LaAlO_3$ has turned up some unexpected elastic relaxation phenomena in addition to the standard strain/order parameter coupling behaviour expected on the basis of Landau theory. They show that the $Pm\bar{3}m \leftrightarrow R\bar{3}c$ phase transition is far from being the simple, improper ferroelastic, soft optic mode transition that it first appeared to be. The full story involves fluctuations above T_c which give rise to softening of acoustic modes with different symmetry, and tails in excess physical properties up to ~860 K. The transition itself is marked by an abrupt increase in acoustic dissipation at frequencies as widely separated at ~1 and $\sim 10^5$ Hz. This dissipation diminishes with falling temperature in a manner which could be understood in terms of domain wall freezing. Below the freezing interval, however, additional elastic and anelastic anomalies have been found which also appear to be related to the high temperature phase transition. The last of the relaxation processes occurs at ~60 K, and the low temperature effects seem to account for the unusual range of saturation temperatures previously found in $LaAlO_3$ (Carpenter *et al* 2009a). There is evidence for incipient instabilities which, if induced more fully by appropriate chemical doping, say, might give rise to piezoelectric or ferroelectric properties. These bear potential analogies with the phenomenologically rich low temperature behaviour of $SrTiO_3$.

For the moment, the working hypothesis in relation to superattenuation of acoustic resonance between ~350 K and T_c is that it has an extrinsic origin related to local bowing of twin walls. This result is at least consistent with the remarkable mobility of twin walls in $LaAlO_3$ known from other studies, even though the details appear to be different. Important additional questions then arise as to the length scales at which twin walls can move, the difference between twin wall roughening and migration, the interaction of mobile walls with phonons, and the local processes by which wall mobility is influenced at a local scale by defects in general or oxygen vacancies in particular. By way of contrast, it is proposed that the low temperature dissipation and softening effects have an intrinsic origin (Carpenter *et al* 2009a). The extent to which dynamical disordering of atomic positions, twin wall mediated dissipation and central peak effects are related to each other remains to be ascertained, but they all appear to be related to the $Pm\bar{3}m \leftrightarrow R\bar{3}c$ transition.

One of the original motivations for investigating the anelastic properties of perovskites, particularly with respect to the dynamics of twin wall motion, was due to the possible attenuation of seismic waves by $(Mg, Fe)SiO_3$ and $CaSiO_3$ perovskite in the earth's lower mantle. Experience of orthorhombic perovskite with $Pnma$ symmetry suggests that their twin walls are typically immobile under the influence of applied stresses at ~1 MHz (Walsh *et al* 2008, McKnight *et al* 2009a, 2009b) but, if only one order parameter operates, such as in tetragonal and rhombohedral forms with octahedral tilting, the twin walls can be highly mobile. Quantitative determination of anelasticity maps of the form shown in figures 10 and 12 for a range of different perovskites should allow the influence of different mechanisms to be systematized as functions of temperature, pressure, stress and frequency. According to the results presented here, there is a real possibility that significant attenuation could occur even at low applied stresses and frequencies. Essentially the same issues arise in the consideration of dissipation behaviour of piezoelectric or ferroelectric ceramics at much higher frequencies.

Not many spectroscopies operate in the region of 0.1–2 MHz and yet this appears to be a particularly sensitive frequency range over which to investigate both extrinsic and intrinsic aspects of relaxational phenomena associated with phase transitions in perovskites. In principle, it should be possible to use this approach to investigate the role of a range of factors, such as oxygen fugacity, chemical dopants and magnetic or electric fields, to address the more general question of how to engineer relaxation properties of ferroic and multiferroic technological ceramics.

Acknowledgments

Elasticity measurements on $LaAlO_3$ have been supported by The Natural Environment Research Council of Great Britain, first under grant no. NER/A/S/2000/01055 and subsequently under grant no. NE/B505738/1 (to MAC). We also thank Ekhard Salje and Richard Harrison for many fruitful and informative discussions.

References

Ashby M F 1972 *Acta Metallogr.* **20** 887–97
Axe J D and Shirane G 1970 *Phys. Rev.* B **1** 342–8
Axe J D, Shirane G and Müller K A 1969 *Phys. Rev.* **183** 820–3
Bourim E M, Tanaka H, Gabbay M, Fantozzi G and Cheng B L 2002 *J. Appl. Phys.* **91** 6662–9
Cao W and Barsch G R 1988 *Phys. Rev.* B **38** 7947–58
Carpenter M A 2007 *Am. Mineral.* **92** 309–27
Carpenter M A, Buckley A, Taylor P A, McKnight R E A and Darling T W 2010a *J. Phys.: Condens. Matter* **22** 035406
Carpenter M A, Darling T W, Bass J D, Lakshtanov D L, Sinogeikin S V and Jacobsen S D 2006 *EOS Trans. Am. Geophys. Union.* **87** (abstract MR34A-01)
Carpenter M A and Salje E K H 1998 *Eur. J. Mineral.* **10** 693–812
Carpenter M A, Sinogeikin S V and Bass J D 2010b *J. Phys.: Condens. Matter* **22** 035404
Carpenter M A, Sinogeikin S V, Bass J D, Lakshtanov D L and Jacobsen S D 2010c *J. Phys.: Condens. Matter* **22** 035403
Chen X, Sichelschmidt O, Kleemann W, Petracic O, Binek Ch, Sousa J B, Cardoso S and Freitas P P 2002 *Phys. Rev. Lett.* **89** 137203
Chen X B, Li C H, Ding Y, Zhang Z F, Shen H M, Zhu J S and Wang Y N 2000 *Phys. Status Solidi* a **179** 455–61
Chrosch J and Salje E K H 1999 *J. Appl. Phys.* **85** 722–7
Combs J A and Yip S 1983 *Phys. Rev.* B **28** 6873–85
Cummins H Z 1979 *Phil. Trans. R. Soc.* A **293** 393–405
Daraktchiev M, Harrison R J, Mountstevens E H and Redfern S A T 2006 *Mater. Sci. Eng.* A **442** 199–203

Daraktchiev M, Salje E K H, Lee W T and Redfern S A T 2007 *Phys. Rev.* B **75** 134102
Fossum J O 1985 *J. Phys. C: Solid State Phys.* **18** 5531–48
Gesi K, Axe J D, Shirane G and Linz A 1972 *Phys. Rev.* B **5** 1933–41
Glatz A, Nattermann T and Pokrovsky V 2003 *Phys. Rev. Lett.* **90** 047201
Harrison R J and Redfern S A T 2002 *Phys. Earth Planet. Inter.* **134** 253–72
Harrison R J, Redfern S A T and Bismayer U 2004a *Mineral. Mag.* **68** 839–52
Harrison R J, Redfern S A T, Buckley A and Salje E K H 2004b *J. Appl. Phys.* **95** 1706–17
Harrison R J, Redfern S A T and Salje E K H 2004c *Phys. Rev.* B **69** 144101
Harrison R J, Redfern S A T and Street J 2003 *Am. Mineral.* **88** 574–82
Hayward S A, Morrison F D, Redfern S A T, Salje E K H, Scott J F, Knight K S, Tarantino S, Glazer A M, Shuvaeva V, Daniel P, Zhang M and Carpenter M A 2005 *Phys. Rev.* B **72** 054110
Höchli U T 1972 *Phys. Rev.* B **6** 1814–23
Huang Y N, Li X, Ding Y, Wang Y N, Shen H M, Zhang Z F, Fang C S, Zhuo S H and Fung P C W 1997 *Phys. Rev.* B **55** 16159–67
Huang Y N, Wang Y N and Shen H M 1992 *Phys. Rev.* B **46** 3290–5
Kityk A V, Schranz W, Sondergeld P, Havlik D, Salje E K H and Scott J F 2000a *Phys. Rev.* B **61** 946–56
Kityk A V, Schranz W, Sondergeld P, Havlik D, Salje E K H and Scott J F 2000b *Europhys. Lett.* **50** 41–7
Kjems J K, Shirane G, Müller K A and Scheel H J 1973 *Phys. Rev.* B **8** 1119–24
Lakes R S 2004 *Rev. Sci. Instrum.* **75** 797–810
Landau L D and Khalatnikov I M 1954 *Dokl. Akad. Nauk SSSR* **96** 469–72
Lee T, Lakes R S and Lal A 2000 *Rev. Sci. Instrum.* **71** 2855–61
Lee W T, Salje E K H, Goncalves-Ferreira L, Daraktchiev M and Bismayer U 2006 *Phys. Rev.* B **73** 214110
Leisure R G and Willis F A 1997 *J. Phys.: Condens. Matter* **9** 6001–29
Lemanov V V, Gridnev S V and Ukhin E V 2002 *Phys. Solid State* **44** 1106–15
Lüthi B and Rehwald W 1981 *Top. Curr. Phys.* **23** 131–84
Lyuksyutov I F, Nattermann T and Pokrovsky V 1999 *Phys. Rev.* B **59** 4260–72
Maynard J 1996 *Phys. Today* **49** 26–31
McKnight R E A, Carpenter M A, Darling T W, Buckley A and Taylor P A 2007 *Am. Mineral.* **92** 1665–72
McKnight R E A, Howard C J and Carpenter M A 2009a *J. Phys.: Condens. Matter* **21** 015901
McKnight R E A, Kennedy B J, Zhou Q and Carpenter M A 2009b *J. Phys.: Condens. Matter* **21** 015902
McKnight R E A, Moxon T, Buckley A, Taylor P A, Darling T W and Carpenter M A 2008 *J. Phys.: Condens. Matter* **20** 075229
Migliori A, Darling T W, Baiardo J P and Freibert F 2001 *Handbook of Elastic Properties of Solids, Liquids and Gases* ed M Levy, H Bass and R Stern (New York: Academic) p 239
Migliori A and Maynard J D 2005 *Rev. Sci. Instrum.* **76** 121301
Migliori A and Sarrao J L 1997 *Resonant Ultrasound Spectroscopy: Applications to Physics, Materials Measurements and Nondestructive Evaluation* (New York: Wiley)
Migliori A, Sarrao J L, Visscher W M, Bell T M, Lei M, Fisk Z and Leisure R G 1993 *Physica* B **183** 1–24
Mueller V, Shchur Y, Beige H, Mattauch S, Glinnemann J and Heger G 2002 *Phys. Rev.* B **65** 134102
Natterman T, Pokrovsky V and Vinokur V M 2001 *Phys. Rev. Lett.* **87** 197005
Nowick A S and Berry B S 1972 *Anelastic Relaxation in Crystalline Solids* (New York: Academic)
Nye J F 1985 *Physical Properties of Crystals* (Oxford: Oxford University Press)
Ogi H, Fukunaga M, Hirao M and Ledbetter H 2004 *Phys. Rev.* B **69** 024104
Postnikov V S, Pavlov V S and Turkov S V 1970 *J. Phys. Chem. Solids* **31** 1785–91
Pytte E 1970 *Phys. Rev.* B **1** 924–30
Pytte E 1971 *Structural Phase Transitions and Soft Modes* (*NATO ASI, Norway*) ed E J Samuelsen, E Anderson and J Feder (Oslo: Scandinavian University Books) p 151
Rehwald W 1970 *Solid State Commun.* **8** 1483–5
Rehwald W 1971 *Phys. Kondens. Mater.* **14** 21–36
Rehwald W 1973 *Adv. Phys.* **22** 721–55
Salje E K H 1990 *Phase Transitions in Ferroelastic and Co-Elastic Crystals* (Cambridge: Cambridge University Press)
Salje E K H and Ishibashi Y 1996 *J. Phys.: Condens. Matter* **8** 8477–95
Salje E K H and Zhang H 2009 *J. Phys.: Condens. Matter* **21** 035901
Schranz W and Kityk A V 2008 *Ferroelectrics* **375** 178–86
Schranz W, Tröster A, Kityk A V, Sondergeld P and Salje E K H 2003 *Europhys. Lett.* **62** 512–8
Schranz W, Sondergeld P, Kityk A V and Salje E K H 1999 *Phase Transit.* **69** 61–76
Schreuer J, Thybaut C, Prestat M, Stade J and Haussühl S 2003 *Proc. IEEE Ultrason. Symp.* **2003** 196–9
Schreuer J and Thybaut C 2005 *Proc. IEEE Ultrason. Symp.* **2005** 695–8
Walsh J N, Taylor P A, Buckley A, Darling T W, Schreuer J and Carpenter M A 2008 *Phys. Earth Planet. Inter.* **167** 110–7
Wang C, Fang Q F, Shi Y and Zhu Z G 2001 *Mater. Res. Bull.* **36** 2657–65
Wang C, Redfern S A T, Daraktchiev M and Harrison R J 2006 *Appl. Phys. Lett.* **89** 152906
Wang C Q, Wang Q F and Zhu Z G 2002 *J. Phys. D: Appl. Phys.* **35** 1545–9
Wang Y N and Huang Y N 1994 *J. Alloys Compounds* **211/212** 356–60
Wang Y N, Huang Y N, Shen H M and Zhang Z K 1996 *J. Physique Coll.* **6** C8–505
Wang Y N, Tian W, Huang Y N, Yan F, Shan H M, Zhu J S and Zhang Z F 2000 *Phase Transit.* **72** 57–80
Wenyuan S, Huimin S, Yening W and Baosheng L 1985 *J. Physique Coll.* **46** C10–609
Yao W, Cummins H Z and Bruce R H 1981 *Phys. Rev.* B **24** 424–44
Yening W, Wenyuan S, Xiaohua C, Huimin S and Baosheng L 1987 *Phys. Status Solidi* a **102** 279–85
Zadler B J, le Rousseau J H L, Scales J A and Smith M L 2004 *Geophys. J. Int.* **156** 154–69